

1 **Australian fire emissions of carbon monoxide estimated**
2 **by global biomass burning inventories: variability and**
3 **observational constraints**

4 **M. J. Desservettaz^{1,2*}, J. A. Fisher¹, A. K. Luhar², M. T. Woodhouse², B.**
5 **Bukosa³, R. R. Buchholz⁴, C. Wiedinmyer⁵, D. W. Griffith¹, P. B. Krummel²,**
6 **N. B. Jones¹, and J. W. Greenslade^{1†}**

7 ¹Centre for Atmospheric Chemistry, School of Earth, Atmospheric and Life Sciences, University of
8 Wollongong, Wollongong, NSW, Australia

9 ²Climate Science Centre, CSIRO Oceans & Atmosphere, Aspendale, Victoria, Australia

10 ³National Institute of Water and Atmospheric Research, Wellington, New Zealand

11 ⁴Atmospheric Chemistry Observations & Modeling Laboratory, National Center for Atmospheric
12 Research, Boulder CO, USA

13 ⁵Cooperative Institute for Research in Environmental Sciences, University of Colorado Boulder, Boulder,
14 CO, USA

15 **Key Points:**

- 16 • GFED4s and QFED2.4 outperform FINN1.5, especially in northern savanna re-
17 gions
- 18 • ACCESS-UKCA provides a better CO simulation near fresh emissions, while GEOS-
19 Chem better captures variability in remote measurements
- 20 • Sparsity and locations of Australian ground-based measurements offer limited con-
21 straints on Australian fire emissions in global models

*Now at the Climate & Atmosphere Research Centre, The Cyprus Institute, Nicosia, Cyprus

†Now at the Bureau of Meteorology, Melbourne, VIC., Australia

Corresponding author: M. J. Desservettaz, m.desservettaz@cyi.ac.cy

Corresponding author: J. A. Fisher, jennyf@uow.edu.au

Abstract

Australian fires are a primary driver of variability in Australian atmospheric composition and contribute significantly to regional and global carbon budgets. However, biomass burning emissions from Australia remain highly uncertain. In this work, we use surface in situ, ground-based total column and satellite total column observations to evaluate the ability of two global models (GEOS-Chem and ACCESS-UKCA) and three global biomass burning emission inventories (FINN1.5, GFED4s, and QFED2.4) to simulate carbon monoxide (CO) in the Australian atmosphere. We find that emissions from northern Australia savanna fires are substantially lower in FINN1.5 than in the other inventories. Model simulations driven by FINN1.5 are unable to reproduce either the magnitude or the variability of observed CO in northern Australia. The remaining two inventories perform similarly in reproducing the observed variability, although the larger emissions in QFED2.4 combined with an existing high bias in the southern hemisphere background lead to large CO biases. We therefore recommend GFED4s as the best option of the three for global modelling studies with focus on Australia or the southern hemisphere. Near fresh fire emissions, the higher resolution ACCESS-UKCA model is better able to simulate surface CO than GEOS-Chem, while GEOS-Chem captures more of the observed variability in the total column and remote surface air measurements. We also show that existing observations in Australia can only partially constrain global model estimates of biomass burning. Continuous measurements in fire-prone parts of Australia are needed, along with updates to global biomass burning inventories that are validated with Australian data.

Plain Language Summary

Biomass burning inventories estimate the distribution and abundance of gases emitted to the atmosphere from fires. In this study, we found that three popular fire emission inventories (GFED, FINN, and QFED) predict very different emissions of the gas carbon monoxide (CO) from fires in Australia. To determine which inventory is best for Australia, we fed those emissions into global atmospheric models that combine the emissions with the chemistry and movement of gases in the atmosphere to predict the abundance of atmospheric gases, including CO. We compared the predictions to measurements in the real atmosphere. We found that two of the inventories (GFED and QFED) are better suited for Australian studies than the third (FINN), which failed to capture much of the annual variation in measured CO levels. To further the outcomes of this study, more ground-based measurements are needed in Australia, particularly in the northern half of the continent where most of the fires normally occur. In addition, the use of atmospheric models with finer resolution would also allow us to make better use of the existing ground-based measurements to judge the reliability of different fire emission inventories.

1 Introduction

Emissions from biomass burning have a large influence on atmospheric composition in the Southern Hemisphere where, relative to the Northern Hemisphere, slash and burn practices, pasture maintenance and accidental fires are more common and emissions from fossil fuels are much lower (Wai et al., 2014). Australia contributes approximately 5-10% to global biomass burning carbon emissions, with contributions from savanna fires in the north and forest fires in the south (Shi et al., 2015; van der Werf et al., 2017; Prosperi et al., 2020). These estimates come from global biomass burning inventories parameterised based on measurements performed almost exclusively outside Australia (Akagi et al., 2011). However, Australian ecosystems are uniquely characterized by a large fraction of eucalyptus vegetation, unlike anywhere else in the world (Gill, 1975), with possible implications for simulation of smoke emissions from Australian fires.

72 The accuracy of global biomass burning emission estimates for Australia has not pre-
 73 viously been evaluated. Here, we perform a suite of global model simulations of atmo-
 74 spheric composition driven by three global biomass burning inventories with differing emis-
 75 sions from Australia. We evaluate these simulations with surface, total column and satel-
 76 lite observations of carbon monoxide (CO), which is a marker of the degree of smoke in
 77 the atmosphere, to assess the fidelity of the inventories as well as the capability of ex-
 78 isting measurements to constrain modelled atmospheric composition in Australia.

79 Global biomass burning emission inventories are widely used as inputs to atmospheric
 80 chemistry models to link emissions to their impacts on atmospheric composition, air qual-
 81 ity, health, and climate. Most inventories calculate the emissions from fires using some
 82 variant of the Seiler and Crutzen algorithm shown in Equation 1 (Seiler & Crutzen, 1980):

$$83 \quad E_i = A \times L \times CC \times EF_i \quad (1)$$

84 where E_i is the estimated mass of species i emitted from biomass burning, calculated
 85 as the product of area burnt (A , area), fuel load (L , mass of fuel per area), combustion
 86 completeness (CC , unitless) and the emission factor for species i (EF_i , mass of species
 87 i emitted per mass of fuel burned). The area burnt is retrieved by satellite imagery. The
 88 fuel load is the amount of combustible vegetation per unit area and can be estimated
 89 from satellite data or be parameterised per vegetation type and region. The combustion
 90 completeness, also referred to as burning efficiency or fractional combustion, is the frac-
 91 tion of the total fuel load that is fully combusted and released to the atmosphere. It is
 92 usually modelled based on the type of vegetation burnt, the estimated fire intensity, and
 93 in some cases the soil moisture content and/or time since the area was last burnt (Giglio
 94 et al., 2013). In some inventories, satellite-derived fire radiative power combined with
 95 regional conversion factors is used as a proxy to estimate the amount of fuel combusted
 96 ($A \times L \times CC$) (Wooster et al., 2005; Darmenov & da Silva, 2015). The emission fac-
 97 tors represent the fraction of the burnt fuel that is emitted as trace gas i . They are de-
 98 rived from laboratory and field measurements conducted using specific fuels or in spe-
 99 cific ecosystems, and are compiled for broad land cover or vegetation type such as sa-
 100 vanna or tropical forest (e.g., Akagi et al., 2011; Andreae & Merlet, 2001).

101 Although most global inventories rely on some form of Equation 1, there are a num-
 102 ber of variations in their input data sources and implementation that lead to significant
 103 differences in emission estimates (Liu et al., 2020; Pan et al., 2020). Inter-inventory dif-
 104 ferences are not globally consistent, and previous work has shown that variability be-
 105 tween inventories is larger for Australia than for most of the rest of the world (Liu et al.,
 106 2020). This variability ultimately leads to large uncertainty in Australian atmospheric
 107 composition as simulated by models that use these inventories as input. Observations
 108 available to constrain these uncertainties are sparse, with only a handful of long-term
 109 trace gas measurement sites (including both remote sensing and surface in situ measure-
 110 ments) spread out across a continent roughly the size of the continental United States.
 111 Perhaps as a result, no previous work has attempted to evaluate the fidelity of different
 112 global inventories for simulating atmospheric composition in the Australian environment.

113 In this work, we address two fundamental questions for understanding the impact
 114 of Australian biomass burning on regional and global atmospheric composition: (1) *How*
 115 *much do current estimates of Australian biomass burning CO emissions vary, and what*
 116 *impact does that variation have on simulated CO abundance?*; and (2) *Are existing ob-*
 117 *servations sufficient to constrain these estimates?* To answer the former, we run a suite
 118 of model simulations using two global atmospheric chemistry models (GEOS-Chem and
 119 ACCESS-UKCA, see acronyms list for full names) with three separate global biomass
 120 burning inventories (GFED4s, FINN1.5, and QFED2.4) and quantify the resultant range
 121 in the magnitude and interannual variability of CO emissions, simulated CO mixing ra-
 122 tios in surface air, and simulated CO total columns. To address the latter, we compare

123 the simulated CO to surface in situ, ground-based total column, and satellite CO obser-
124 vations and evaluate the performance of each simulation. In the following sections, we
125 first describe the biomass burning emission inventories, global models, and measurement
126 datasets (Section 2). We then compare estimates of biomass burning emissions from each
127 of the three inventories for Australia and contextualise these on hemispheric and global
128 scales (Section 3). Finally, we evaluate the CO simulations using the Australian obser-
129 vations and make recommendations as to the most appropriate biomass burning emis-
130 sions to use for simulating Australian atmospheric composition (Section 4).

131 2 Methodology

132 The evaluation was done for the period 2008-2010. This 3-year time frame was se-
133 lected to encompass 2009, the year of the ‘Black Saturday’ event which, until the sum-
134 mer of 2019-2020, was Australia’s worst bushfire disaster on record. This event took place
135 around 7 February 2009 and burnt 4500 km² of forest in the south-eastern state of Vic-
136 toria, claiming 173 lives and destroying more than 3500 buildings (Cruz et al., 2012). This
137 major biomass burning event left a clear fingerprint on both atmospheric measurements
138 and emission estimates (Paton-Walsh et al., 2012; Siddaway & Petelina, 2011). Thus,
139 a 3-year window around the Black Saturday event was simulated to capture the impact
140 of interannual variability on the results.

141 We quantify the relative importance of variability in emission inventories versus
142 variability in chemical transport model by using two global atmospheric chemistry mod-
143 els and three emission inventories. The impact of variability in emission inventories is
144 quantified by running one model (GEOS-Chem) with all three inventories (GFED4s, FINN1.5,
145 and QFED2.4). The impact of model variability is quantified by running both models
146 (GEOS-Chem and ACCESS-UKCA) with the same emission inventory (GFED4s). The
147 inventories and models are described briefly below (Sections 2.1 and 2.2), along with the
148 observations and statistical measures used to evaluate the model simulations (Section
149 2.3). Our analysis uses CO as the trace gas that is both measured at the most Australian
150 observing sites and most sensitive to biomass burning emissions. Preliminary additional
151 evaluation using formaldehyde and ethane (both measured at fewer stations than CO)
152 provided no additional insights and therefore is not discussed further.

153 2.1 Biomass burning emission inventories

154 2.1.1 GFED4s

155 The Global Fire Emissions Database version 4s (GFED4s) biomass burning emis-
156 sions were used in both the GEOS-Chem model with 3-hourly resolution, and in the ACCESS-
157 UKCA model with monthly resolution (models described below). The GFED4s inven-
158 tory is described in detail by van der Werf et al. (2017). In brief, the fuel loading in GFED4s
159 is derived from the Carnegie-Ames-Stanford-Approach (CASA) biogeochemical model
160 (Potter et al., 1993; Field et al., 1995; Randerson et al., 1996). The GFED4 burned area
161 (without small fires) is obtained from the 500 m MODIS Collection 5.1 MCD64A1 burned
162 area product (Giglio et al., 2013). For fires smaller than 21 ha (the size of the 500 m x
163 500 m MODIS pixel), the direct mapping of the burned area is not reliable. Therefore,
164 to account for smaller fires, active fires from MODIS and 500 m x 500 m surface reflectance
165 observations are combined with the MCD64A1 burned area product. The burned area
166 of small fires is calculated by multiplying the number of active fires outside the perime-
167 ter of the MCD64A1 burned area by the ratio of burned area to active fires within the
168 perimeter of the MCD64A1 burned area. The estimate of burned area for each small fire
169 is refined by a correction factor to account for the region, vegetation type and season.
170 Specific details of this approach are given by Randerson et al. (2012).

171 As detailed by van der Werf et al. (2017) and references therein, fuel load and com-
 172 bustion completeness are derived from the carbon cycle aspect inherited from CASA. The
 173 model dynamically adjusts the modelled amount of carbon in different carbon pools (such
 174 as stems, leaves and litter) using the fraction of absorbed photosynthetically active ra-
 175 diation, a dataset derived from measurements by the Advanced Very High Resolution
 176 Radiometer (AVHRR) sensor on-board several satellites. Combustion completeness is
 177 set between minimum and maximum fractions depending on the land cover and then de-
 178 fined within those limits using soil moisture. Land cover types include evergreen needle-
 179 leaf forests, evergreen broadleaf forests, deciduous needleleaf forests, deciduous broadleaf
 180 forests, mixed forests, closed shrublands, open shrublands, woody savannas, savannas,
 181 grasslands and croplands. Emission factors are from the inventory compilation by Akagi
 182 et al. (2011).

183 **2.1.2 FINN1.5**

184 The Fire INventory from NCAR version 1.5 (FINN1.5) biomass burning emissions,
 185 described in detail by Wiedinmyer et al. (2011), were used only as input to GEOS-Chem,
 186 with daily resolution. In FINN, the location and size of fires are derived from satellite
 187 detection of active fires only. Active fires are retrieved from the MODIS Thermal Anoma-
 188 lies Product daily, with a nominal resolution of 1 km². Fires detected with a confidence
 189 level of less than 20% are removed. In the tropics, between 30°N and 30°S, MODIS takes
 190 two days to achieve full coverage. Therefore, fires detected on one day are assumed to
 191 carry over to the following day at half their original size. Because there are two MODIS
 192 instruments, the possibility of double-counting fires is removed by discounting any hot
 193 spot detected within a 1-km radius of an existing fire detection each day.

194 The MODIS Collection 5 Land Cover Type supplies FINN1.5 with the type of veg-
 195 etation burned in each pixel. Fourteen of the sixteen land types in the MODIS dataset
 196 are lumped into six generic land cover classes: boreal forests, tropical forests, temper-
 197 ate forests, woody savannas and shrublands, savannas and grasslands and croplands. The
 198 remaining two, water and ice, are used to filter out any anomalous hot spots. The frac-
 199 tion of tree, non-tree vegetation and bare cover in each pixel is obtained from the MODIS
 200 Vegetation Continuous Fields product. The area burned is assumed to be 1 km² for each
 201 pixel, except for savanna and grassland areas, where it is assumed to be 0.75 km² (due
 202 to the lower vegetation density). The area burned values are further scaled using the MODIS
 203 Vegetation Continuous Field bare cover fraction in each pixel.

204 Fuel loading is set by region and generic land cover class based on Hoelzemann et
 205 al. (2004). For instance, the fuel density for savanna and grassland vegetation in Ocea-
 206 nia is estimated at 245 g m⁻², which is approximately half the density estimated for the
 207 same land cover type in South America (552 g m⁻²). This represents a significant dif-
 208 ference from GFED4s and its dynamically calculated fuel loading. The combustion com-
 209 pleteness is set depending on the tree cover with three options: tree cover below 40%,
 210 tree cover between 40% and 60%, and tree cover higher than 60%. As in GFED4s, emis-
 211 sion factors are from Akagi et al. (2011).

212 **2.1.3 QFED2.4**

213 The Quick Fire Emission Dataset version 2.4 (QFED2.4) biomass burning emis-
 214 sions, described by Darmanov and da Silva (2015), were used only in GEOS-Chem, with
 215 daily resolution. In QFED, emissions are calculated based on fire radiative power, which
 216 quantifies the rate of radiant heat produced by a fire and has been shown to be linearly
 217 related to the mass of fuel consumed in a fire (Wooster, 2002). Fire radiative power and
 218 fire location are obtained from the MODIS Collection 5 Active Fire product (MOD14
 219 and MYD14) and the MODIS Geolocation product (MOD03 and MYD03) with a 1 km²
 220 spatial resolution, up to four times each day. In the case of pixels obscured by clouds,

221 QFED2.4 uses a technique called the sequential approach, which models a predicted value
222 of fire radiative power from a previous measurement in the same pixel. This predicted
223 value is then used to correct the observed fire radiative power with a scalar parameter,
224 which depends on the quality of the sensor’s retrieval.

225 The QFED vegetation map is then used to assign the vegetation type, select the
226 relevant coefficient to convert fire radiative power to mass of dry fuel consumed, and se-
227 lect the relevant emission factors. The QFED vegetation map is derived from the Inter-
228 national Geosphere-Biosphere Programme (IGBP), with improvements of the Brazilian
229 tropical forests by the Brazilian National Institute For Space Research (IGBP-INPE),
230 with 1 km² spatial resolution. The IGBP-INPE 17 land cover types are aggregated into
231 four basic vegetation types used by QFED: tropical forest, extra-tropical forest, savanna
232 and grassland. For each vegetation type, the fire radiative power-to-fuel consumption
233 coefficients are based on comparison to GFEDv2. Emission factors are from Andreae and
234 Merlet (2001), which for CO are ~15% different for extratropical forest fires and almost
235 identical for savanna fires to those reported by Akagi et al. (2011) (as used in the other
236 two inventories).

237 2.2 Chemical Transport Models

238 2.2.1 GEOS-Chem

239 We used the tropospheric chemistry (“tropchem”) simulation of the GEOS-Chem
240 (Bey et al., 2001) chemical transport model version 10-01 ([http://wiki.seas.harvard](http://wiki.seas.harvard.edu/geos-chem/index.php/GEOS-Chem_v10-01)
241 [.edu/geos-chem/index.php/GEOS-Chem_v10-01](http://wiki.seas.harvard.edu/geos-chem/index.php/GEOS-Chem_v10-01)), driven by assimilated meteorologi-
242 cal fields from the NASA Global Modelling and Assimilation Office Goddard Earth Ob-
243 serving System, Version 5 (GEOS-5) reanalysis data product. For global simulations as
244 used here, the native GEOS-5 resolution of 0.5° latitude by 0.667° longitude by 72 ver-
245 tical levels is downgraded for use in GEOS-Chem to 2° latitude by 2.5° longitude by 47
246 vertical levels. The model uses a hybrid sigma pressure vertical grid. The vertical res-
247 olution decreases with height, with up to 38 levels in the troposphere. The tropopause
248 is calculated dynamically, and so the number of levels in the troposphere varies. Only
249 purely stratospheric levels are lumped when downgrading the resolution from 72 to 47
250 vertical levels.

251 The model was run from 2008-2010. A six month spin-up preceded the period of
252 interest to allow the model’s chemistry to reach equilibrium. Model timesteps were 15
253 minutes for convection and transport and 30 minutes for emissions and chemistry. Model
254 output was saved with hourly resolution at the measurement sites and monthly resolu-
255 tion everywhere else.

256 Biomass burning emissions (described above) were emitted into the model surface
257 layer. Anthropogenic emissions were from the Emission Database for Global Atmospheric
258 Research (EDGARv4.2; Olivier et al., 2002) for CO, nitrogen oxides, sulfur dioxide and
259 ammonia and the REanalysis of the TROpospheric chemical composition (RETRO; Rein-
260 hart & Millet, 2011) for volatile organic compounds. These were supplemented with bio-
261 fuel emissions from Yevich and Logan (2003), aircraft emissions from the Aviation Emis-
262 sions Inventory Code (AEIC; Simone et al., 2013) and ship emissions from the Interna-
263 tional Comprehensive Ocean Atmosphere Data Set (ICOADS; Woodruff et al., 2011) for
264 CO and nitrogen oxide and from the Arctic Research of the Composition of the Tropo-
265 sphere from Aircraft and Satellites inventory (ARCTAS; Eyring et al., 2005)) for sulfur
266 dioxide. Biogenic emissions were from the Model of Emissions of Gases and Aerosols from
267 Nature v2.1 (MEGANv2.1; Guenther et al., 2012), calculated online in GEOS-Chem.

268

2.2.2 ACCESS-UKCA

269

270

271

272

273

274

275

276

277

278

We used the ACCESS-UKCA chemistry-climate model, which combines the physical atmosphere from the United Kingdom Met Office’s Unified Model version 8.4 with the UKCA chemistry model (Abraham et al., 2012; Bi et al., 2013; Woodhouse et al., 2015, <http://www.ukca.ac.uk>). In the model setup used here, ACCESS is essentially the same as the Unified Model since the ACCESS-specific ocean and land-surface components are not invoked as the model is run in atmosphere-only mode with prescribed monthly mean sea surface temperature and sea ice fields, and the UM’s original land-surface scheme (Joint UK Land Environment Simulator; JULES) is used. The UKCA configuration used here combines both tropospheric and stratospheric chemistry schemes. The total number of reactions, including aerosol chemistry, is 306 across 86 species.

279

280

281

282

The atmospheric model has a horizontal resolution of 1.875° in longitude and 1.25° in latitude, and 85 staggered terrain-following hybrid-height levels extending from the surface to 85 km. The vertical resolution decreases with height, with the lowest 65 levels (up to ~ 30 km) lying within the troposphere and lower stratosphere.

283

284

285

286

287

The model’s meteorological fields (horizontal wind components and potential temperature) were nudged to ECMWF’s ERA-Interim reanalyses (Dee et al., 2011) on pressure levels in the free troposphere. The model output used here was extracted from a longer model run starting from 1997. Because the model was not run specifically for this work, only monthly mean model output was available.

288

289

290

291

292

293

Biomass burning emissions were from GFED4s (described above) with CO emitted into the model surface layer. Anthropogenic emissions were from the Atmospheric Chemistry and Climate Model Intercomparison Project (ACCMIP; Lamarque et al., 2013). Biogenic emissions were from the MEGAN – Monitoring Atmospheric Composition and Climate project (MEGAN-MACC; Sindelarova et al., 2014). A detailed description of the ACCESS-UKCA simulation as used here is presented in Woodhouse et al. (2015).

294

2.3 Observations

295

296

297

298

299

To evaluate the two atmospheric models over Australia using the three estimates of biomass burning emissions, we used a suite of CO observations from surface in situ data, ground-based total column data, and satellite-based measurements from the Measurements Of Pollution In The Troposphere (MOPITT) instrument onboard NASA’s Earth Observing System Terra spacecraft.

300

301

302

303

304

305

306

307

308

309

310

311

312

313

314

315

316

Figure 1 shows the locations of the four Australian sites where ground-based in situ and/or total column CO observations were available: Darwin (Northern Territory), Cape Ferguson (Queensland), Wollongong (New South Wales), and Cape Grim (Tasmania). Surface in situ data were available for all sites except Wollongong, for which only total column data were consistently available during the study period. At Darwin, surface in situ measurements were made using a Fourier Transform InfraRed (FTIR) spectrometer with 3-minute resolution. The instrumental setup is presented by D. W. T. Griffith et al. (2012). At Cape Ferguson, in situ CO was sampled in flasks with approximately weekly resolution and analysed by gas chromatography with mercuric oxide reduction detector (Langenfelds et al., 2002). At Cape Grim, in situ CO was sampled every 40 minutes by gas chromatography with a mercuric oxide reduction detector (Prinn et al., 2018). The Cape Ferguson data is available from the World Data Centre for Greenhouse Gases (WDCGG), part of the Global Atmospheric Watch program of the World Meteorological Organisation (Krummel et al., 2016). The Cape Grim data were provided directly by the Commonwealth Scientific and Industrial Research Organisation (CSIRO). For comparison to the models, the surface in situ observations were averaged to both hourly and monthly resolution.

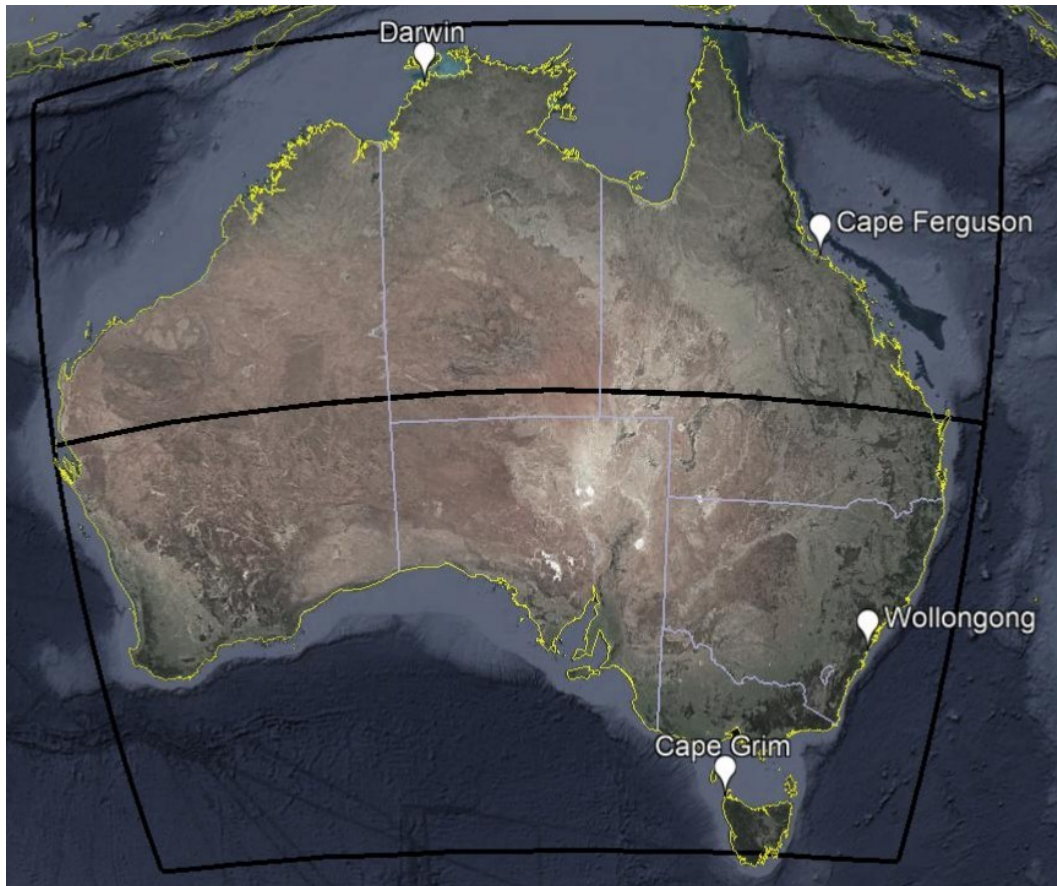


Figure 1. Location of the ground-based measurements sites: Darwin (12.5°S , 130.8°E), Cape Ferguson (19.3°S , 147.1°E), Wollongong (34.4°S , 150.9°E), and Cape Grim (40.7°S , 144.7°E). The black lines delimit the northern and southern Australian regions (separated by 25°S) referred to in this study. Satellite image from Google Earth (Landsat/Copernicus).

317 Ground-based measurements of total column CO were made at Wollongong and
 318 Darwin using high-resolution solar FTIR spectrometers. Total column CO measurements
 319 were from the Network for the Detection of Atmospheric Composition Change (NDACC;
 320 <http://www.ndsc.ncep.noaa.gov/>) at Wollongong and the Total Column Carbon Ob-
 321 serving Network (TCCON; <http://www.tccon.caltech.edu/>) at Darwin (D. Griffith
 322 et al., 2014)). The time resolution of both instruments is approximately 1 minute, and
 323 measurements are only made under cloud free conditions. For comparison to GEOS-Chem
 324 model output, the total column datasets, including averaging kernels and a priori pro-
 325 files provided as part of the dataset, were averaged to hourly time resolution, and com-
 326 parisons were made only for hours with available measurements. Modelled vertical pro-
 327 files were extrapolated to the instrument’s vertical levels and converted to partial columns.
 328 Instrumental averaging kernels and a priori profiles were then applied to the model par-
 329 tial columns and the smoothed partial columns summed to calculate smoothed model
 330 total columns that account for instrument sensitivity (Rodgers & Connor, 2003). Like-
 331 wise, the total column datasets were also averaged monthly to account for instrument
 332 sensitivity when comparing with the ACCESS-UKCA model output (available at monthly
 333 resolution only).

334 To provide broader regional context, the models were also compared to MOPITT
 335 Version 7 level 3 monthly data, obtained from the NASA data archive ([ftp://15ei101](ftp://15ei101.larc.nasa.gov/MOPITT/MOP03JM.007)
 336 [.larc.nasa.gov/MOPITT/MOP03JM.007](ftp://15ei101.larc.nasa.gov/MOPITT/MOP03JM.007), (NASA/LARC/SD/ASDC, n.d.)). The joint/multispectral
 337 TIR-NIR product was used, which, with the inclusion of solar reflectance, improves near-
 338 surface retrievals (Worden et al., 2010). The level 3 product of the nadir-sounding MO-
 339 PITT instrument has a $1^\circ \times 1^\circ$ horizontal resolution with global coverage over approx-
 340 imately three days (Drummond & Mand, 1996; Deeter et al., 2017; Emmons et al., 2009).
 341 The CO retrieval provides one to two independent pieces of information in the vertical.
 342 MOPITT uses correlation infrared radiometry, a technique that uses a cell on-board the
 343 instrument containing CO as reference. The internal length and pressure of this cell are
 344 modulated to gain spectral information. Buchholz et al. (2017) validated MOPITT CO
 345 using data from the NDACC network, including from Wollongong. They found MOPITT
 346 to slightly overestimate CO compared to ground-based FTIR (<10%) but did not find
 347 any significant latitude-dependent bias.

348 Similar to the ground-based total columns, MOPITT instrumental averaging ker-
 349 nels and a priori profiles were applied to the model output to account for instrumental
 350 sensitivity. MOPITT data and smoothed model output were then averaged spatially over
 351 the northern and southern Australia regions shown in Figure 1. The 25°S latitude was
 352 chosen as the boundary between the northern and southern Australia regions following
 353 Buchholz et al. (2018) as: (1) it marks a dramatic change in rainfall and fire hotspot dis-
 354 tributions (Russell-Smith et al., 2007); (2) it roughly coincides with the Tropic of Capri-
 355 corn that divides tropical from temperate regions; and (3) it separates Australia’s more
 356 populous south from the sparsely populated north (about 85% of the Australian popu-
 357 lation lives south of 25°S).

358 For all datasets, model-observation agreement was quantified by calculating the mean
 359 bias (MB , Equation 2) and the Pearson correlation coefficient (r) for each simulation com-
 360 pared to the relevant measurement dataset:

$$361 \quad MB = \frac{\sum_{i=1}^N (M_i - O_i)}{N} \quad (2)$$

362 where N is the number of data points and M and O are the model and observed
 363 parameters respectively. The mean bias represents the average difference between the
 364 model output and observation. The correlation coefficient quantifies the strength of the
 365 linearity between model outputs and observation and is indicative of the model ability
 366 to reproduce the observed variability.

Table 1. Australian biomass burning CO emission estimates.

| Region | Year | CO emissions (Tg) | | |
|---------------------------------|------|-------------------|--------|---------|
| | | FINN1.5 | GFED4s | QFED2.4 |
| Northern Australia ^a | 2008 | 1.2 | 8.9 | 16. |
| | 2009 | 2.1 | 13. | 22. |
| | 2010 | 0.7 | 4.8 | 8.7 |
| Southern Australia ^b | 2008 | 0.5 | 0.8 | 1.7 |
| | 2009 | 1.8 | 3.0 | 3.0 |
| | 2010 | 1.8 | 1.2 | 2.4 |
| Australian total | 2008 | 1.7 | 9.7 | 18. |
| | 2009 | 3.9 | 16. | 25. |
| | 2010 | 2.5 | 6.0 | 11. |

^aNorth of 25°S^bSouth of 25°S

3 Biomass Burning Emission Estimates

3.1 Australian Emissions

Table 1 presents the total estimated CO emissions from Australian biomass burning as calculated from the GEOS-Chem output with each inventory in each simulation year, separated into northern and southern Australian contributions (Figure 1). The spatial distribution of CO emissions is shown in Figure 2 for the year 2009 as an example, with total emissions from GFED4s (Fig. 2a) compared to FINN1.5 (Fig. 2b) and QFED2.4 (Fig. 2c). All three inventories show emissions from savanna fires in the north and forest fires in the southeast, with the northern savanna fires the dominant emission source.

The total annual Australian biomass burning CO emissions vary by up to an order of magnitude between inventories. Emissions are lowest in FINN1.5 (1.7-3.9 Tg), followed by GFED4s (6-16 Tg), with the largest emissions from QFED2.4 (11-25 Tg). Liu et al. (2020) compared five biomass burning inventories, including the three of this study, and also found FINN (v1.5) and QFED (v2.5r1) to be the extreme cases for Australia when averaged over 2003-2016. Figure 2 shows that emissions from FINN1.5 are lower than GFED4s throughout Australia, while emissions from QFED2.4 are higher than GFED4s over the savanna regions but lower over the forest regions (both tropical and temperate).

The inventories differ most significantly for the savanna fires in northern Australia. In both GFED4s and QFED2.4, the northern Australian emissions dominate the total Australian emissions budget, responsible for 4.8-13 Tg CO (76-89% of the Australian total) in GFED4s and 8.7-22 Tg (79-88% of the Australian total) in QFED2.4. These results are consistent with previous estimates that 83% of Australian biomass burning emissions originate from savanna fires (Shi et al., 2015). FINN1.5 emissions, on the other hand, are very low in northern Australia at only 0.7-2.1 Tg of CO. The savanna fire emissions in FINN1.5 dominate the total Australian fire emissions only in 2008; in other years they account for only 28-53% of the total.

The inventories also differ in their representations of interannual variability. Summed over both regions, FINN1.5 emissions are lowest in 2008, while GFED4s and QFED2.4 both show the lowest emissions in 2010. All three inventories show the largest emissions in 2009, both in the southern Australia region affected by the Black Saturday fires and in the northern Australia savanna region.

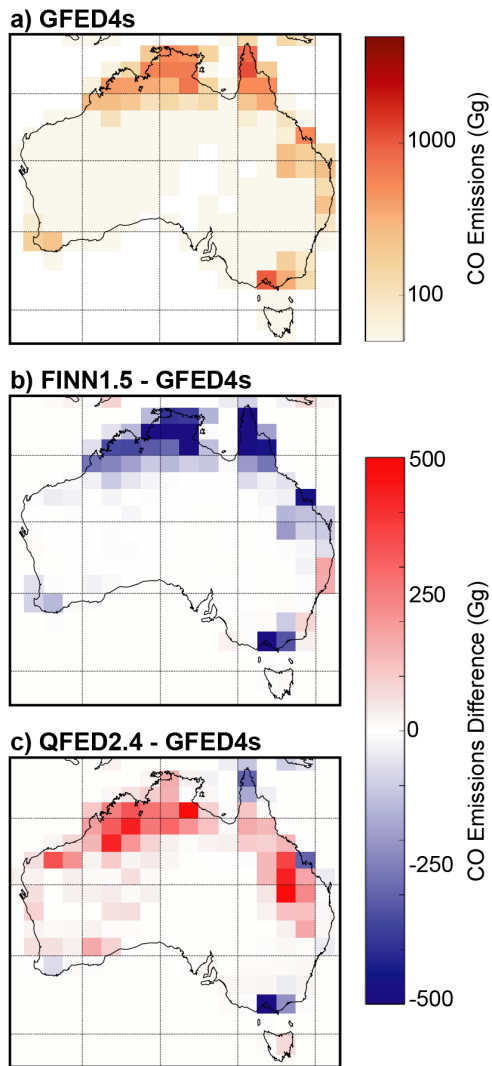


Figure 2. (a) CO emissions (Gg) over Australia in 2009 from GFED4s, along with the absolute differences between (b) FINN1.5 and GFED4s and (c) QFED2.5 and GFED4s.

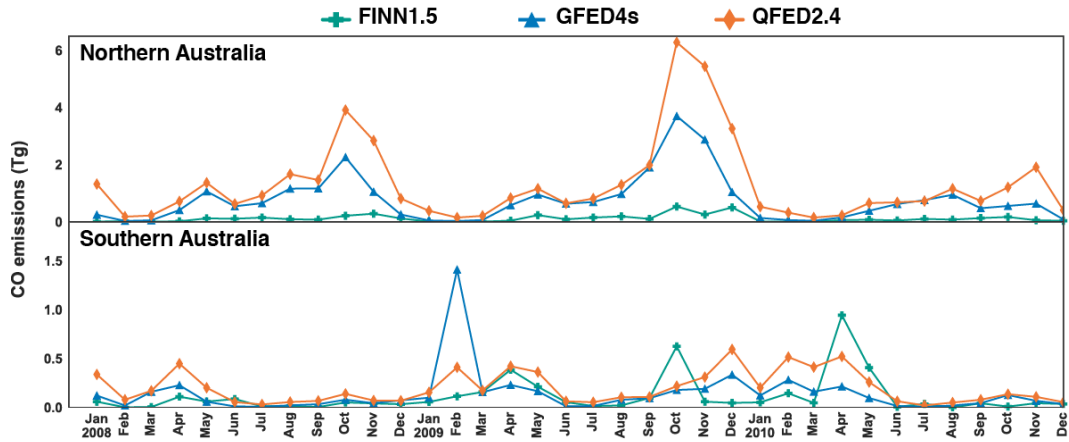


Figure 3. Biomass burning CO emissions (Tg) for northern (top) and southern (bottom) Australia as estimated by FINN1.5 (teal), GFED4s (blue), and QFED2.4 (orange) from January 2008 to December 2010. Note the difference in scales between the top and bottom panels.

398 Figure 3 shows the time series of monthly mean CO emissions estimated by each
 399 inventory for northern and southern Australia (note the difference in scales). In north-
 400 ern Australia, GFED4s and QFED2.4 show that the largest emission peaks occur from
 401 September to December each year during the tropical dry season (Edwards et al., 2006),
 402 although only QFED2.4 shows a distinct peak in the latter half of 2010. FINN1.5 does
 403 not show any northern Australia seasonal CO increase in 2008 and 2010 and only a very
 404 small enhancement in 2009.

405 In southern Australia, CO emissions peak during austral summer (December to Febru-
 406 ary), as shown in Figure 3. GFED4s and to a lesser extent QFED2.4 show a peak in south-
 407 ern Australia CO emissions in February 2009, coincident with the Black Saturday event.
 408 FINN1.5 does not show any enhancement during this event but does show significant peaks
 409 in October 2009 and March 2010 that are not seen in the other inventories.

410 3.2 Continental, Hemispheric and Global Emissions

411 To contextualise the Australian emissions, we also compare the inventory estimates
 412 for other Southern Hemisphere continents and at hemispheric and global scales. Table
 413 2 presents annual total biomass burning CO emissions estimates for Australia, Africa,
 414 South America and South-East Asia (all south of the equator), the Southern Hemisphere,
 415 and the global total. Figure 4 shows the time series of the emission estimates for each
 416 region.

417 The three inventories agree well at the hemispheric scale, with mean annual emis-
 418 sions of 177 Tg (FINN1.5), 141 Tg (GFED4s), and 188 Tg (QFED2.4) in the Southern
 419 Hemisphere. However, this agreement masks differences at the continental scale that op-
 420 erate in different directions. While Australian emissions were significantly lower in FINN1.5
 421 than in other inventories, South American emissions are higher in FINN1.5 for two of
 422 the three years. The three inventories agree best over Southern Hemisphere Africa, with
 423 GFED4s and QFED2.4 agreeing within 5-15% of one another while FINN1.5 is 15-45%
 424 lower than GFED4s.

425 Figure 4 shows that there are seasonal and interannual differences between the in-
 426 ventories. For the Southern Hemisphere Africa region, the start of the burning season
 427 is one month later in FINN1.5 than in the other inventories. In GFED4s and QFED2.4,

Table 2. Annual CO emissions (Tg) obtained from the three inventories for Southern Hemisphere regions and the globe.^a

| | | CO emissions (Tg) | | |
|------------------------------------|-------------|-------------------|--------|---------|
| | | FINN1.5 | GFED4s | QFED2.4 |
| Australia | 2008 | 1.6 | 10 | 18 |
| | 2009 | 3.9 | 16 | 25 |
| | 2010 | 2.5 | 6.0 | 11 |
| Africa^b | 2008 | 79 | 96 | 107 |
| | 2009 | 66 | 95 | 101 |
| | 2010 | 56 | 103 | 117 |
| South America^b | 2008 | 70 | 33 | 51 |
| | 2009 | 51 | 17 | 35 |
| | 2010 | 67 | 102 | 81 |
| South-East Asia^b | 2008 | 3.9 | 2.7 | 5.5 |
| | 2009 | 17 | 49 | 8.1 |
| | 2010 | 4.0 | 1.6 | 5.8 |
| Southern Hemisphere | 2008 | 141 | 154 | 181 |
| | 2009 | 178 | 138 | 170 |
| | 2010 | 213 | 130 | 214 |
| Global | 2008 | 327 | 298 | 365 |
| | 2009 | 297 | 318 | 335 |
| | 2010 | 299 | 353 | 369 |

^a Emissions are calculated from the GEOS-Chem output^b South of the equator

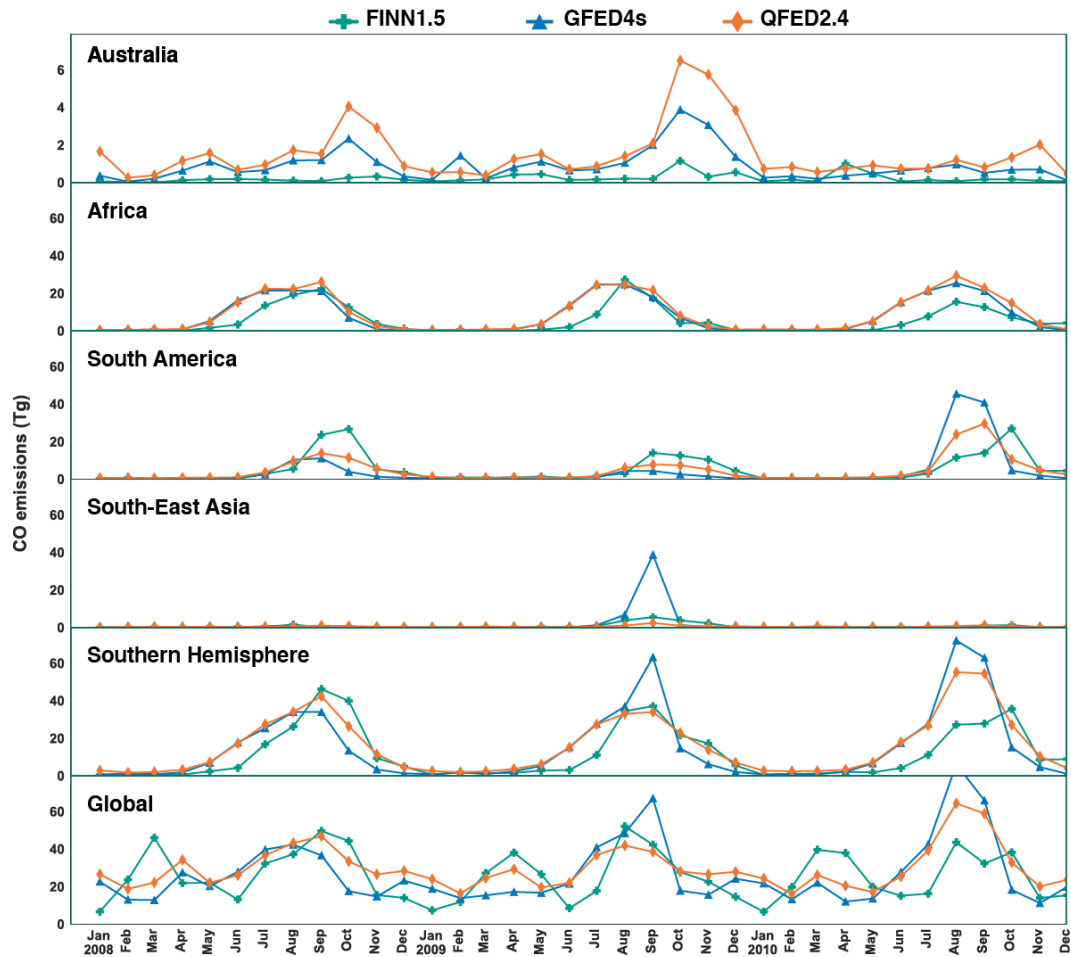


Figure 4. CO emissions (Tg) from biomass burning in (top to bottom) Australia, Africa, South America, South-East Asia, the Southern Hemisphere and the global total, as estimated by FINN1.5 (teal), GFED4s (blue) and QFED2.4 (orange) from January 2008 to December 2010. For the continental totals, only the regions south of the equator are included. Note the scale differences between Australia and all other regions.

there is little year-to-year difference in the seasonal emission maximum, whereas FINN1.5 predicts lower peak emissions in 2010 than in prior years.

Compared with Africa, the inventories show more interannual variability in the Southern Hemisphere South America region. All three inventories predict lower emissions in 2009 and higher emissions in 2010 (coincident with major fires in Bolivia and Brazil; Lewis et al., 2011), with 2008 intermediate in GFED4s and QFED2.4 but on par with 2010 in FINN1.5. In general, QFED2.4 and GFED4s emissions estimates in this region are quite similar in both magnitude and timing, although the annual decline from September to October is more rapid in GFED4s. During the South American fires in August-September 2010, GFED4s estimates are roughly 30% higher than those from QFED2.4. As was the case in Africa, the start of the South American burning season is delayed in FINN1.5 relative to the other inventories. FINN1.5 does not appear to capture the large August-September 2010 emission enhancement associated with the Bolivian and Brazilian fires, but does show an unexplained large peak in October 2010.

As shown in Figure 4, the variability on the hemispheric scale is almost exclusively driven by the variability in the African and South American emissions. One exception is the GFED4s peak in September 2009, which can be attributed to Indonesian fires. In general, emissions from Australia are dwarfed by those from Africa and South America, with Australia responsible for between 1% (FINN1.5 in 2008 and 2010) and 15% (QFED2.4 in 2009) of the hemispheric total. This small contribution combined with the long CO atmospheric lifetime (2 to 6 months; Khalil & Rasmussen, 1984) complicates the evaluation of the inventories using Australian CO observations, as will be discussed below.

4 Simulated CO at Australian measurement sites

As shown in the previous Section, the estimates of Australian biomass burning emissions differ substantially between the GFED4s, FINN1.5, and QFED2.4 inventories. In this section, we evaluate the impact of these different emission estimates on simulated CO mixing ratios in the Australian region. We compare the model output to a suite of Australian atmospheric observations (described in Section 2.3) to test whether existing observations are sufficient to constrain the biomass burning emission estimates and, if so, determine which inventories provide the most accurate simulation of CO observed over Australia.

4.1 Northern Australia

We first compare simulated CO to surface in situ mixing ratios observed at Darwin and Cape Ferguson and to total column observations at Darwin (see Figure 1 for locations). Model evaluation using surface in situ observations provides information about model/inventory ability to reproduce specific fire events if these occur in the vicinity of the site, as most emissions (including those from low-intensity fires) are released within the planetary boundary layer. This is especially true at Darwin, which is located in close proximity to savanna fires and has previously been shown to regularly sample smoke from these fires (Hurst, Griffith, & Cook, 1994; Hurst, Griffith, Carras, et al., 1994; Cook et al., 1995; Paton-Walsh et al., 2010; Desservettaz et al., 2017). Cape Ferguson, on the other hand, is a more remote site, and surface in situ measurements here tend to be more representative of northern Australia background air (Buchholz et al., 2016). Evaluation using the total column data provides complementary information on model simulation of regional air mass characteristics, with the column measurements less sensitive to local emissions and variations in the boundary layer mixing height than measurements made at the surface (Deutscher et al., 2010; Zeng et al., 2015). The integrated nature of the total column measurements can make them more appropriate for comparison to global models with coarse resolution (including those used here), but also makes them more sensitive to variations in emissions from distant sources.

Table 3. Mean bias between the modelled and measured surface CO mixing ratios and total columns in northern Australia.^a

| | FINN1.5 | GEOS-Chem QFED2.4 | GFED4s | ACCESS-UKCA^b GFED4s |
|------------------------------------------------------------------------------|----------------|------------------------------|---------------|-------------------------------------------|
| Surface In Situ (ppbv) | | | | |
| Darwin (observed mean = 157.6) | | | | |
| Hourly data | -69.6 (-44%) | -36.9 (-23%) | -50.4 (-32%) | |
| Monthly mean | -69.4 (-44%) | -36.8 (-23%) | -50.0 (-32%) | -2.5 (-2%) |
| Cape Ferguson | | | | |
| Hourly data | 10.6 (17%) | 24.1 (38%) | 12.9 (21%) | |
| Monthly mean | 12.3 (20%) | 24.0 (38%) | 14.6 (23%) | 16.1 (26%) |
| Total Column (10^{18} molec cm^{-2}) | | | | |
| Darwin (observed mean = 1.52) | | | | |
| Hourly data | 0.079 (5%) | 0.269 (18%) | 0.153 (10%) | |
| Monthly mean | 0.057 (4%) | 0.247 (16%) | 0.133 (9%) | 0.248 (16%) |
| MOPITT^c (observed mean = 1.45) | | | | |
| Monthly mean | 0.102 (7%) | 0.236 (17%) | 0.126 (9%) | 0.138 (10%) |

^a See Figure 1 for locations.^b Only monthly mean model output is available for ACCESS-UKCA.^c Averaged over the full northern Australia region shown in Figure 1.

478 We first quantify overall simulation performance using the mean bias relative to
479 each observed dataset. Table 3 shows the mean bias of each simulation (GEOS-Chem
480 with all three inventories and ACCESS-UKCA with GFED4s) in northern Australia. For
481 each dataset, the bias has been calculated using both the original hourly data (shown
482 in Figure 5) and the data averaged to monthly resolution, with only the latter available
483 for the ACCESS-UKCA output. The mean bias relative to MOPITT satellite observa-
484 tions averaged over the full northern Australia region is also included in Table 3.

485 The mean biases in Table 3 provide a consistent picture: the models underestimate
486 CO in the vicinity of fresh local emissions (Darwin surface in situ) but overestimate re-
487 gional background CO (Cape Ferguson surface in situ, Darwin and MOPITT total columns).
488 The three GEOS-Chem simulations show results consistent with the differences between
489 emission inventories described in Section 3: simulated CO is lowest with FINN1.5 fol-
490 lowed by GFED4s and then QFED2.4. This means that at sites where the model is bi-
491 ased high, the mean bias is smallest for GEOS-Chem/FINN1.5 and largest for GEOS-
492 Chem/QFED2.4, while at sites where the model is biased low, the opposite is true. When
493 compared to the Darwin surface in situ measurements, the difference between the two
494 models (GEOS-Chem and ACCESS-UKCA) with the same inventory (GFED4s) is strik-
495 ing: while the GEOS-Chem/GFED4s simulation underestimates observed CO by more
496 than 30%, the ACCESS-UKCA/GFED4s simulation is within 2% of the observed mean.
497 The reason for this difference will be explored in detail below. For the other measure-
498 ments, the differences between models (ACCESS-UKCA/GFED4s vs. GEOS-Chem/GFED4s)
499 is smaller than the difference between inventories when using the same model (GEOS-
500 Chem).

501 The mean biases tell us little about the relative suitability of each inventory to re-
502 produce true Australian CO. For most of the year, Australian CO burdens are dominated
503 by secondary production from oxidation of methane and other volatile organic compounds

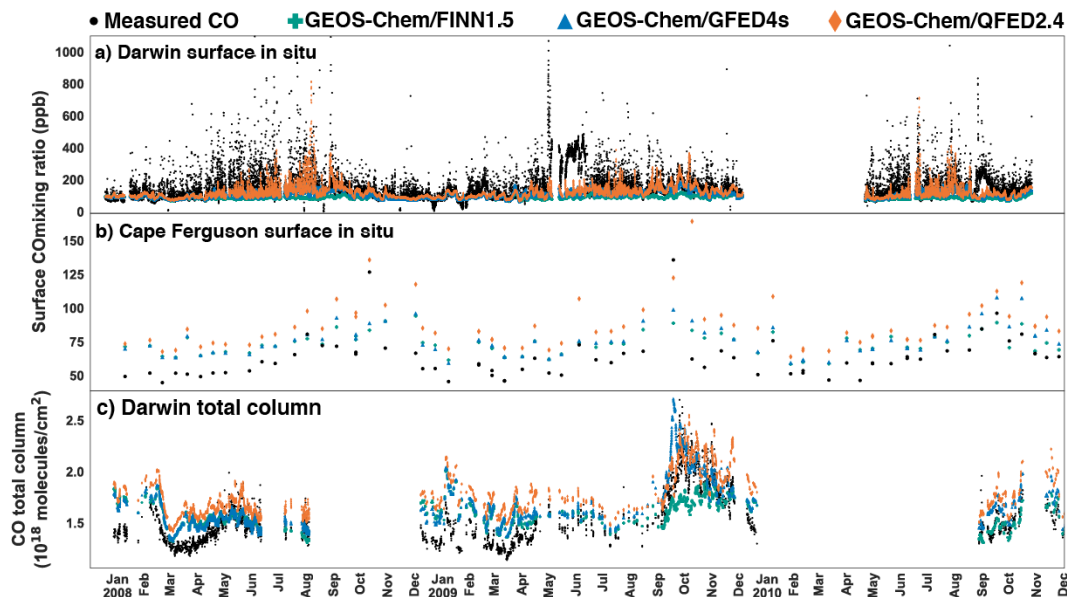


Figure 5. Time series of hourly measured (black) and simulated (colours) (a,b) surface and (c) total column CO in northern Australia. Note that ACCESS-UKCA output was not available at hourly resolution and is therefore not included in this figure. A similar figure averaged to monthly resolution can be found in the supplement.

504 (Fisher et al., 2017). While some of these source compounds are associated with biomass
 505 burning, most are from biogenic emissions (Zeng et al., 2015). As a result, the overall
 506 mean CO values in the models are largely driven by sources other than biomass burn-
 507 ing. Considering the documented general high CO bias in model simulations (Naik et
 508 al., 2013), a lower bias caused by a change in fire emission inventory might actually re-
 509 flect a compensating effect of insufficient emissions. Therefore, mean biases are not an
 510 adequate test of inventory performance for biomass burning episodes.

511 Model variability, on the other hand, is more significantly influenced by biomass
 512 burning emissions due to the seasonal and episodic nature of this source (Edwards et al.,
 513 2006). GEOS-Chem tagged CO simulations from Fisher et al. (2017) (available only for
 514 2009-2010) confirm these assumptions hold at the observation sites used here: secondary
 515 CO is responsible for 70-90% of simulated CO throughout the year, while primary biomass
 516 burning emissions drive the annual cycle and interannual variability (see Figures S1-S3
 517 in the supplement).

518 We therefore focus our analysis on model ability to reproduce variability rather than
 519 mean values. The relative ability of each simulation to reproduce the observed variabil-
 520 ity is quantified using the correlation coefficient r between each simulation and the mea-
 521 surements. Correlation coefficients calculated using both the hourly data (where avail-
 522 able) and the monthly means are provided in Table 4. Model ability to reproduce ob-
 523 served variability at monthly timescales is also shown qualitatively in Figure 6, which
 524 compares the measured monthly mean CO to the simulated monthly mean after remov-
 525 ing the mean bias. An equivalent figure without the mean bias subtracted can be found
 526 in the supplement (Figure S4).

527 At Darwin, the GEOS-Chem simulations show limited ability to reproduce the ob-
 528 served variability from the surface in situ record. For the hourly observations, the cor-
 529 relation coefficients are $r=0.25$ for GEOS-Chem/QFED2.4 and $r=0.22$ for GEOS-Chem/GFED4s,

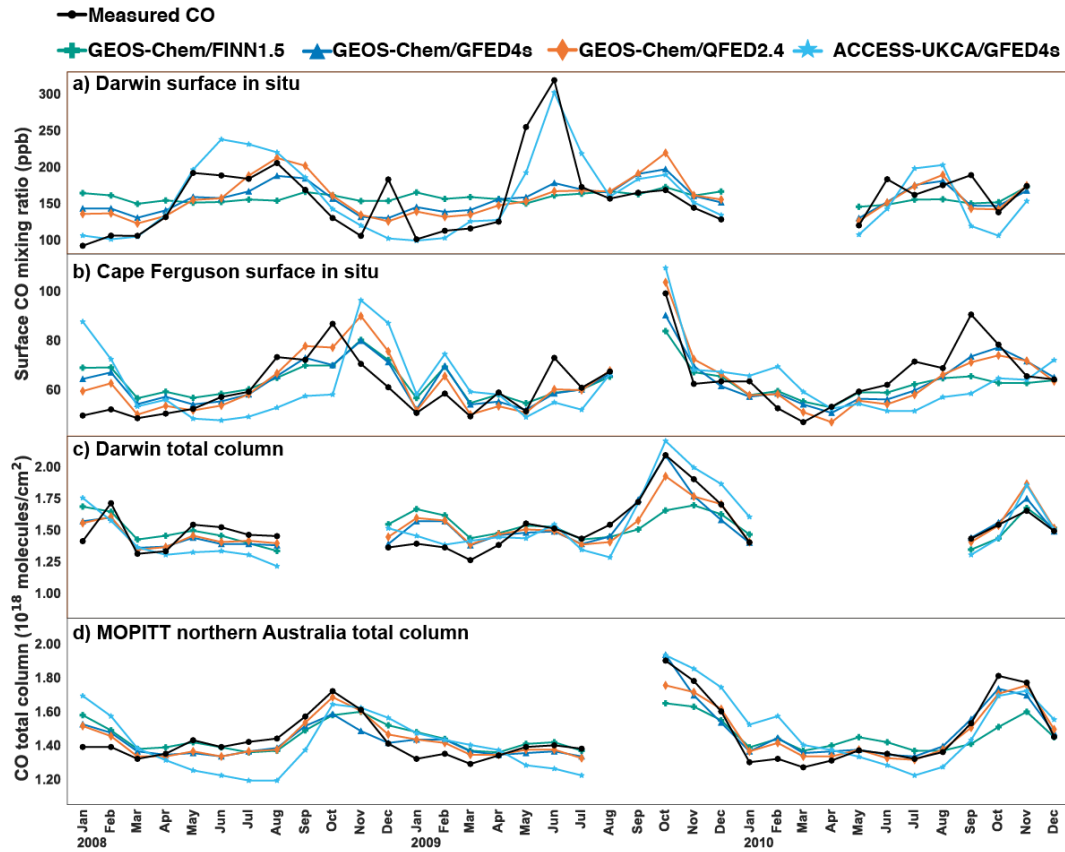


Figure 6. Monthly averaged (a,b) surface CO mixing ratio and (c,d) total column CO in northern Australia from measurements (black) and simulations (colours). The mean bias of each simulation has been removed to better highlight differences in variability.

Table 4. Correlation coefficients (r) between the modelled and measured surface CO mixing ratios and total columns in northern Australia.^a

| | GEOS-Chem | | | ACCESS-UKCA ^b |
|---------------------------|-----------|---------|--------|--------------------------|
| | FINN1.5 | QFED2.4 | GFED4s | GFED4s |
| Surface In Situ | | | | |
| Darwin | | | | |
| Hourly data | <0.01 | 0.25 | 0.22 | |
| Monthly mean | -0.09 | 0.44 | 0.53 | 0.80 |
| Cape Ferguson | | | | |
| Hourly data | 0.67 | 0.70 | 0.73 | |
| Monthly mean | 0.62 | 0.79 | 0.76 | 0.31 |
| Total Column | | | | |
| Darwin | | | | |
| Hourly data | 0.56 | 0.80 | 0.82 | |
| Monthly mean | 0.50 | 0.80 | 0.86 | 0.77 |
| MOPITT^c | | | | |
| Monthly mean | 0.80 | 0.94 | 0.91 | 0.70 |

^a See Figure 1 for locations.^b Only monthly mean model output is available for ACCESS-UKCA.^c Averaged over the full northern Australia region shown in Figure 1.

530 implying the model captures at most $\sim 6\%$ of the observed variability (defined as r^2). For
531 these simulations, the correlation coefficients improve when both observation and model
532 are averaged to monthly resolution, reproducing about 20% (QFED2.4) to 30% (GFED4s)
533 of the observed monthly variability. This improvement shows that GEOS-Chem is bet-
534 ter able to simulate the mean annual cycle than the individual events sampled in the hourly
535 data. With FINN1.5, the GEOS-Chem simulation is uncorrelated with the hourly data
536 and weakly anti-correlated with the monthly mean data, suggesting major deficiencies
537 in the ability of FINN1.5 to estimate either the magnitude or variability of fire emissions
538 near Darwin.

539 ACCESS-UKCA performs significantly better for Darwin surface CO than all GEOS-
540 Chem simulations, including when both models are driven by GFED4s emissions, with
541 ACCESS-UKCA able to reproduce more than twice as much of the seasonal variability
542 as GEOS-Chem/GFED4s. Figure 6 shows a much larger seasonal enhancement simu-
543 lated by ACCESS-UKCA than by GEOS-Chem, particularly in 2009. The more accu-
544 rate simulation of the seasonal peak by ACCESS-UKCA also explains the much smaller
545 bias in ACCESS-UKCA relative to GEOS-Chem noted earlier (Table 3).

546 The large discrepancy between ACCESS-UKCA/GFED4s and GEOS-Chem/GFED4s
547 is surprising given that we expect most of the CO seasonality at Darwin to be driven by
548 biomass burning emissions (Edwards et al., 2006; Paton-Walsh et al., 2010), and both
549 simulations use the same emission inventory. Other differences between the models that
550 could influence simulation of the surface CO mixing ratio include horizontal resolution,
551 land fraction (emittable area) in the grid cell containing Darwin, vertical injection height,
552 and differences in meteorological fields caused by the use of different reanalysis products.
553 We test the influence of each of these on simulated CO using the existing model output.
554 We find that nearly all of the difference can be explained by differences in horizontal re-
555 solution between the models, as shown in Figure 7. Re-mapping the ACCESS-UKCA out-

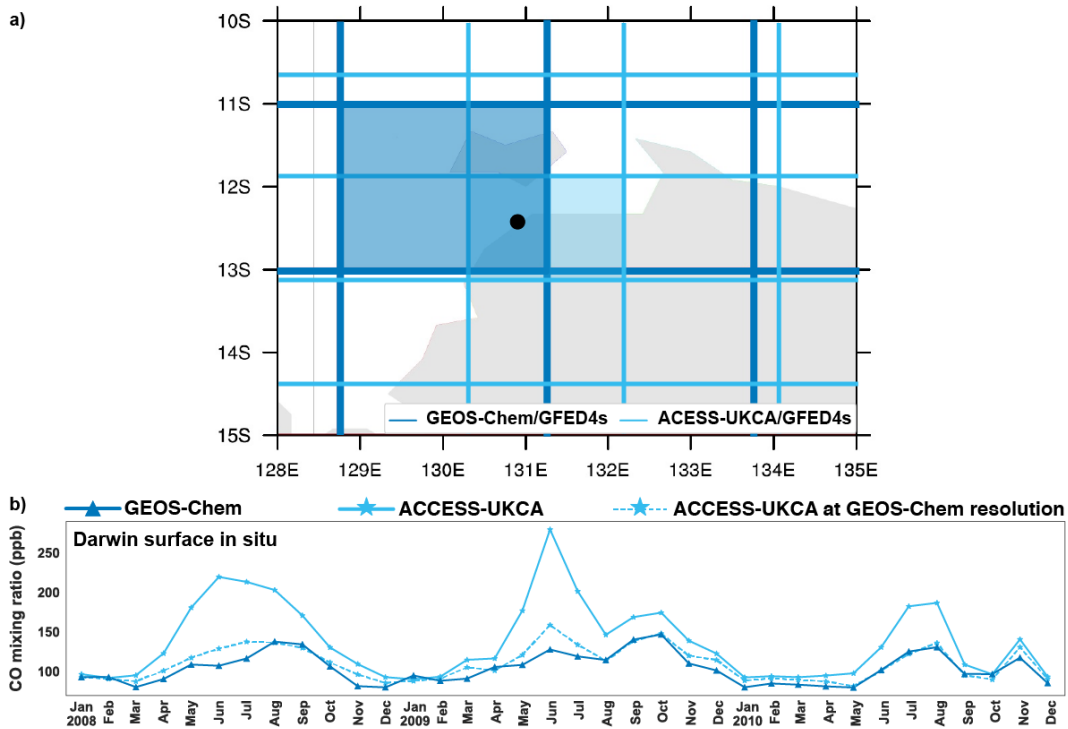


Figure 7. (a) GEOS-Chem (dark blue) and ACCESS-UKCA (light blue) model grid box locations in the region near Darwin. The black circle indicates the Darwin measurement site and the shaded boxes show the grid cells sampled in each model to represent Darwin. (b) Time series of modelled CO in Darwin surface air from GEOS-Chem (solid dark blue), ACCESS-UKCA (solid light blue), and ACCESS-UKCA re-mapped to the GEOS-Chem resolution (dashed light blue) using the Climate Data Operators (CDO) first-order conservative remapping function (remap-con).

556 put from the native $1.25^\circ \times 1.875^\circ$ resolution to the coarser $2^\circ \times 2.5^\circ$ GEOS-Chem res-
 557 resolution substantially reduces the peak simulated CO as the emissions are diluted over
 558 the larger area, effectively eliminating the difference between the two models. Meanwhile,
 559 as shown in the supplement (Figures S5-S6), there appears to be little impact from the
 560 land versus ocean fraction in the Darwin grid cell (tested by sampling GEOS-Chem us-
 561 ing grid cells with higher land fraction to the south and east) or from emission injection
 562 height and mixing (tested by comparing the simulated vertical distribution between mod-
 563 els). These results highlight the strong horizontal resolution dependence of near-source
 564 observation-model comparisons and suggest a more robust test of the inventories at Dar-
 565 win would require running a high-resolution model forced by the different inventories.

566 The Cape Ferguson surface in situ site is located substantially further from local
 567 emissions. As a result, the differences in model resolution are less important here. All
 568 simulations appear to have a 1-month lag in the timing of peak CO in 2008 and 2010
 569 (Figure 6), which is a few months later at Cape Ferguson than at Darwin. However, miss-
 570 ing data in 2009 and a generally sparse observation record due to the infrequent sam-
 571 pling (Figure 5) make it difficult to reliably determine the timing of the seasonal peak.
 572 ACCESS-UKCA performs notably worse ($r=0.31$) than any of the GEOS-Chem simu-
 573 lations ($r=0.62-0.79$) in simulating the annual cycle at Cape Ferguson. Amongst the GEOS-
 574 Chem simulations, the model best simulates the observed monthly means when using
 575 GFED4s and QFED2.4, reproducing 58% and 62% of the variability, respectively. With

576 the mean biases removed, the GEOS-Chem/FINN1.5 simulation is nearly identical to
 577 GEOS-Chem/GFED4s for most of the simulation period but misses the seasonal increase
 578 in the latter half of 2010 (Figure S4), reducing the correlation with the observations.

579 The total column observations are much less sensitive to nearby emissions than the
 580 surface measurements, as discussed previously. At Darwin, all simulations except GEOS-
 581 Chem/FINN1.5 are able to reproduce the majority of the variability observed in both
 582 the hourly data and the monthly means, with correlation coefficients of $r=0.77-0.86$. All
 583 four simulations reproduce to some extent the peak total column CO observed in 2009,
 584 which occurs a few months later in the total column (October) than at the surface (June).
 585 However, the simulated peak is much smaller in the GEOS-Chem/FINN1.5 simulation
 586 than in the other simulations or the observations, leading to a weaker correlation. Al-
 587 though the GEOS-Chem CO total columns at Darwin are typically lower with GFED4s
 588 than QFED2.4, the situation is reversed during the 2009 peak (Figure S4), presumably
 589 due to the much larger emissions from the 2009 Indonesian fires in GFED4s than in the
 590 other inventories (Figure 4). Overall, the GEOS-Chem/GFED4s simulation outperforms
 591 both the GEOS-Chem/QFED2.4 and the ACCESS-UKCA/GFED4s simulation in terms
 592 of both mean bias (Table 3) and correlation (Table 4).

593 Comparison to the MOPITT satellite total columns averaged over northern Aus-
 594 tralia captures the seasonal cycle, but shows high bias in all simulations (Table 3), par-
 595 ticularly from January to April (Figure S4). Consistent with the other comparisons, GEOS-
 596 Chem/FINN1.5 underestimates the seasonal CO peak. As seen previously for the Dar-
 597 win total column data, GEOS-Chem/GFED4s provides the best simulation of the MO-
 598 PITT data when considering both the mean bias (Table 3) and the correlation (Table
 599 4), with this simulation able to reproduce 88% of the observed seasonal variability. Mean-
 600 while, ACCESS-UKCA/GFED4s overestimates the strength of the seasonal cycle (Fig-
 601 ure 6), degrading the correlation (Table 4).

602 4.2 Southern Australia

603 We perform a similar analysis using the datasets from southern Australia (Cape
 604 Grim surface in situ and Wollongong total column, plus MOPITT regional averages).
 605 Inventory analysis using these measurements comes with several caveats outlined here.
 606 Cape Grim is a remote site on the north-west coast of Tasmania, designed to primar-
 607 ily sample baseline or background air from the Southern Ocean region (Law et al., 2010;
 608 Loh et al., 2015). Therefore, differences at Cape Grim between the three GEOS-Chem
 609 simulations driven by the different inventories are generally more indicative of transported
 610 emissions from Africa and South America than local emissions from southern Australia.
 611 Meanwhile, Wollongong is a semi-urban site located on the east coast of New South Wales
 612 roughly 100 km south of Sydney. The site does occasionally sample smoke from local fires
 613 (e.g., Rea et al., 2016) but is also sensitive to anthropogenic, biogenic, and long-range
 614 transported biomass burning sources (Buchholz et al., 2016; Fisher et al., 2017; Lieschke
 615 et al., 2019).

616 The mean biases of each simulation relative to the Cape Grim and Wollongong mea-
 617 surements and the MOPITT satellite data (averaged over southern Australia) are shown
 618 in Table 5. Consistent with the results for the remote sites in northern Australia, all sim-
 619 ulations show a high bias relative to the observations. As before, amongst the GEOS-
 620 Chem simulations, the magnitude of the bias correlates with the magnitude of the emis-
 621 sions, with the largest biases using QFED2.4 and the smallest using FINN1.5. Compar-
 622 ison to the hourly observations (Figure 8) shows that GEOS-Chem clearly overestimates
 623 the background CO amounts, irrespective of the emission inventory. Comparing the monthly
 624 means (shown in Figure S7 in the supplement) suggests ACCESS-UKCA provides a bet-
 625 ter simulation of the southern mid-latitude background than GEOS-Chem, with a smaller
 626 mean bias at Cape Grim and almost no bias at Wollongong (Table 5). As discussed pre-

Table 5. Mean bias between the modelled and measured surface CO mixing ratios and total columns in southern Australia.^a

| | FINN1.5 | GEOS-Chem QFED2.4 | GFED4s | ACCESS-UKCA ^b GFED4s |
|------------------------------------------------------------------------------|-------------|----------------------|-------------|------------------------------------|
| Surface In Situ (ppbv) | | | | |
| Cape Grim (observed mean = 55.8) | | | | |
| Hourly data | 18.3 (33%) | 26.3 (47%) | 18.6 (33%) | |
| Monthly mean | 18.2 (33%) | 26.2 (47%) | 18.6 (33%) | 12.0 (22%) |
| Total Column (10^{18} molec cm^{-2}) | | | | |
| Wollongong (observed mean = 1.36) | | | | |
| Hourly data | 0.128 (9%) | 0.307 (23%) | 0.159 (12%) | |
| Monthly mean | 0.134 (10%) | 0.314 (23%) | 0.164 (12%) | 0.025 (2%) |
| MOPITT^c (observed mean = 1.35) | | | | |
| Monthly mean | 0.068 (5%) | 0.207 (15%) | 0.093 (7%) | 0.006 (<1%) |

^a See Figure 1 for locations.^b Only monthly mean model output is available for ACCESS-UKCA.^c Averaged over the full southern Australia region shown in Figure 1.

627 viously, biases in the simulations reflect a combination of bias in the model background
628 and inventory-driven differences; we therefore again focus on simulated variability (as
629 as represented by the correlation coefficient, r) to better differentiate the impacts of the
630 different inventories.

631 Comparison of the observed and simulated variability (after subtracting the model
632 mean biases) is shown in Figure 9. In the observational record, the only clear signal of
633 the February 2009 Black Saturday event is seen in the Wollongong total columns. All
634 four simulations capture this event to some extent, although only GEOS-Chem/GFED4s
635 accurately simulates the strength of the enhancement (consistent with the emissions com-
636 parisons shown in Figure 3). In the models, the February 2009 event is also seen at Cape
637 Grim by the two simulations that use the GFED4s emissions, but there is no equivalent
638 enhancement in the observations or the other simulations. The fact that the anomalous
639 enhancement is simulated by both models but only when using GFED4s implies it is caused
640 by the strength of the emissions in GFED4s rather than by anomalous transport to the
641 Cape Grim site. It is possible that the GFED4s inventory overestimates the emissions
642 associated with the Black Saturday event, causing the February 2009 bias at Cape Grim.
643 The more accurate simulation of the event at Wollongong could reflect compensating bi-
644 ases from emissions overestimates and plume dilution at the coarse model resolution (Eastham
645 & Jacob, 2017; Rastigejev et al., 2010), given the significant distance from the fires to
646 the Wollongong site. It should also be noted that while there has been recent progress
647 in modelling smoke plume injection height (as reviewed by Paugam et al., 2016), both
648 models used in this study inject all fire emissions at ground level, adding further uncer-
649 tainty to plume dispersion.

650 Other observed variations can also be seen in the Cape Grim record in Figure 9,
651 including an enhancement in surface CO in March-April 2008. The event is visible in all
652 simulations and in the observations, although the FINN1.5 and GFED4s simulations un-
653 derestimate the duration and ACCESS-UKCA greatly overestimates the magnitude. The
654 March-April 2008 enhancement is likely due to a large fire in the Tarkine Wilderness,
655 which burned nearly 20,000 hectares in northwest Tasmania near the Cape Grim site (BrisbaneTimes,

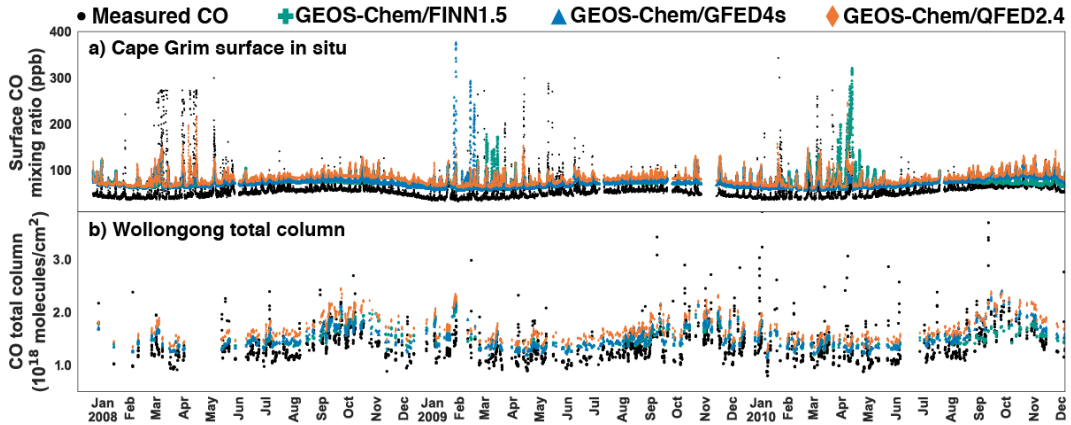


Figure 8. Time series of hourly measured (black) and simulated (colours) (a) surface and (b) total column CO in southern Australia. Note that ACCESS-UKCA output was not available at hourly resolution and is therefore not included in this figure. A similar figure averaged to monthly resolution can be found in the supplement (Fig S7).

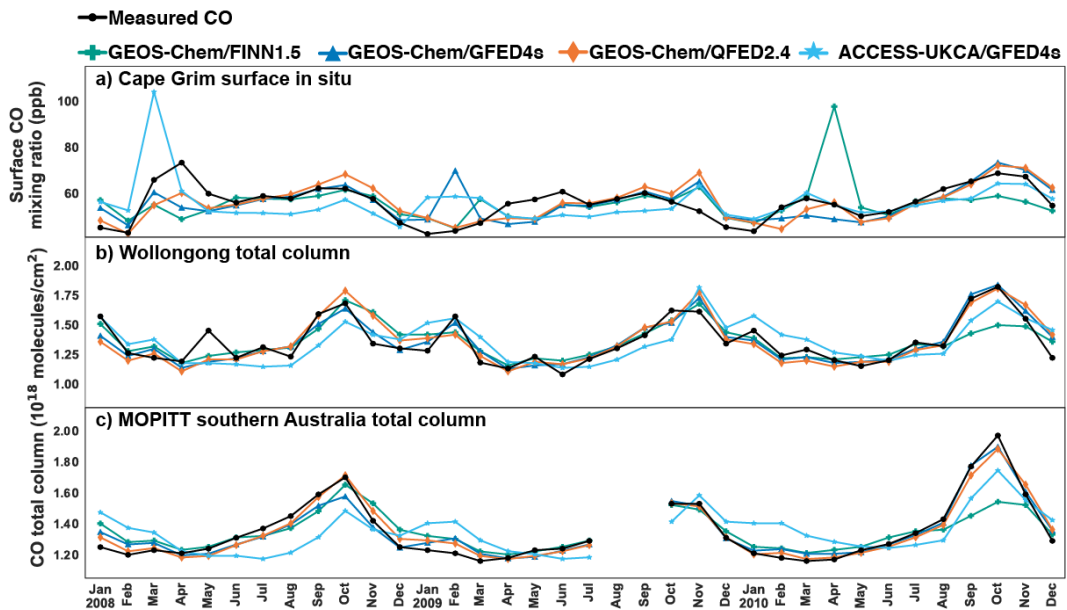


Figure 9. Monthly averaged (a) surface CO mixing ratio and (b,c) total column CO in southern Australia from measurements (black) and simulated (colours). The mean bias of each simulation has been removed to better highlight differences in variability.

Table 6. Correlation coefficients (r) between the modelled and measured surface CO mixing ratios and total columns in southern Australia.^a

| | GEOS-Chem | | ACCESS-UKCA ^b | |
|---------------------------|-----------|---------|--------------------------|--------|
| | FINN1.5 | QFED2.4 | GFED4s | GFED4s |
| Surface In Situ | | | | |
| Cape Grim | | | | |
| Hourly data | 0.39 | 0.66 | 0.48 | |
| Monthly mean | 0.22 | 0.72 | 0.51 | 0.35 |
| Total Column | | | | |
| Wollongong | | | | |
| Hourly data | 0.58 | 0.65 | 0.66 | |
| Monthly mean | 0.78 | 0.86 | 0.90 | 0.70 |
| MOPITT^c | | | | |
| Monthly mean | 0.86 | 0.98 | 0.97 | 0.64 |

^a See Figure 1 for locations.^b Only monthly mean model output is available for ACCESS-UKCA.^c Averaged over the full southern Australia region shown in Figure 1.

2008). The much larger enhancement in the ACCESS-UKCA/GFED4s simulation than in the equivalent GEOS-Chem/GFED4s simulation likely reflects the same resolution dependence seen for the local fires at Darwin; however, in this case GFED4s appears to overestimate the emissions leading to the high bias in the better resolved ACCESS-UKCA simulation. The GEOS-Chem/FINN1.5 simulation at Cape Grim shows a similarly large enhancement in April 2010 that is not seen in the observations or the other simulations. The magnitude of the peak again suggests local emissions; however, in this case there is no evidence of nearby fires and the enhancement appears to be the consequence of erroneous emissions in the FINN1.5 inventory, consistent with the emissions shown in Figure 3.

Overall, GEOS-Chem driven by QFED2.4 provides the best simulation of the observed variability at Cape Grim, with a correlation coefficient of $r \approx 0.7$ (compared to 0.2-0.5 for the other simulations), as shown in Table 6. At Wollongong, there is less difference between simulations in terms of ability to reproduce observed variability. GEOS-Chem simulations driven by QFED2.4 and GFED4s perform similarly to one another, with correlation coefficients of 0.65-0.66 against the observed hourly data and 0.86-0.90 against the observed monthly means. Figure 9 shows that the monthly variability simulated by GEOS-Chem/FINN1.5 is nearly identical to that from the other GEOS-Chem simulations, except in late 2010 when GEOS-Chem/FINN1.5 underestimates the seasonal peak (leading to the weaker correlation in Table 6). The source attribution in the Supplement (Figure S2) suggests this peak is associated with the South American fires, implying FINN1.5 underestimates emissions from these fires (as discussed previously in Section 3). Despite having the lowest bias (Table 5), the ACCESS-UKCA simulation is the least correlated with the Wollongong observations ($r=0.70$) but still captures roughly half of the observed monthly variability.

The MOPITT data for southern Australia provide little additional insight. As at Wollongong, the GEOS-Chem simulations driven by GFED4s and QFED2.4 provide the best simulation of the annual cycle. As the MOPITT data have been averaged over the entire southern Australia region, they primarily reflect the southern mid-latitude CO back-

685 ground with little influence from primary biomass burning emissions (Figure S3). The
 686 exception is the influence of the South American fires in late 2010, when the FINN1.5
 687 underestimate is again evident. As at Wollongong, ACCESS-UKCA provides the poor-
 688 est simulation of the annual cycle, with model overestimates in the first half of the year
 689 and underestimates in the second half that are not seen in the GEOS-Chem simulations.
 690 A similar pattern was seen in the ACCESS-UKCA comparison to MOPITT in north-
 691 ern Australia (Figure 6) and is almost certainly due to model chemistry (secondary CO
 692 production and/or loss) rather than any direct impact of the biomass burning emissions.

693 4.3 Statistical Summary & Recommendations

694 Figure 10 summarises the simulation-measurement comparisons using a Taylor di-
 695 agram to simultaneously compare the different simulations on the basis of their corre-
 696 lation coefficients, root mean squared error (RMSE) and standard deviation relative to
 697 the observations. The RMSE values are calculated after removing the mean bias. The
 698 standard deviations are normalised to the relevant observational dataset such that val-
 699 ues greater than 1 represent greater variability in the simulations than was observed. The
 700 Taylor diagram provides a condensed visual representation of the overall capabilities of
 701 the four simulations. An ideal simulation would have an RMSE of 0.0, normalised stan-
 702 dard deviation of 1.0, and correlation coefficient of 1.0, indicated on the figure as the black
 703 circle labeled “obs”. The closer each point sits to the “obs” marker, the better that sim-
 704 ulation represents the observations. We use the monthly mean data here to enable com-
 705 parison between GEOS-Chem and ACCESS-UKCA simulations on equal footing.

706 Consistent with the results presented previously, the models perform best when com-
 707 pared to the regionally-averaged satellite observations followed by the ground-based to-
 708 tal column observations, with the worst performance relative to the surface in situ mea-
 709 surements. This summary reinforces the point that the coarse resolution models used
 710 here are best suited to interpretation of measurements that represent large spatial scales.
 711 Higher resolution models would be required to more accurately resolve and evaluate emis-
 712 sions at the local scale measured by the surface in situ data.

713 More importantly, Figure 10 shows that the Australian observational record is most
 714 accurately simulated using GEOS-Chem with either GFED4s or QFED2.4 emissions. Our
 715 results suggest that the ACCESS-UKCA simulation, which currently uses only GFED4s
 716 emissions, would not be improved by using the FINN1.5 or QFED2.4 emissions. Instead,
 717 the poorer performance by ACCESS-UKCA than GEOS-Chem/GFED4s (except at the
 718 Darwin surface) may be partly explained by the fact that the ACCESS-UKCA chem-
 719 istry scheme has some limitations compared to GEOS-Chem – for example, ACCESS-
 720 UKCA lumps ethane, ethene and ethyne into ethane and lumps propene into propane;
 721 a generic “NMVOC” (non-methane volatile organic compound) species is used as proxy
 722 for acetaldehyde, and ketone is used as proxy for acetone. These simplifications in or-
 723 ganic compounds will impact CO through secondary production, both in biomass burn-
 724 ing plumes and in background air.

725 Comparison of the three GEOS-Chem simulations suggests that FINN1.5 is not fit-
 726 for-purpose in simulating CO over Australia. Both near-source and downwind observa-
 727 tions in northern Australia imply large errors in FINN1.5 estimates of emissions from
 728 savanna fires, which are virtually non-existent relative to the other inventories (Figure
 729 3). Meanwhile, observations in southern Australia that largely capture the influence of
 730 transported emissions also suggest that FINN1.5 underestimates CO biomass burning
 731 emissions in South America. Liu et al. (2020) previously found that simulations driven
 732 by FINN1.5 also performed poorly relative to other inventories in Indonesia. While their
 733 results were based on fine particulate matter, we expect similar biases would affect sim-
 734 ulation of Indonesian CO emissions, with likely implications for CO transported to north-
 735 ern Australia. We therefore recommend that FINN1.5 not be used for Australian mod-

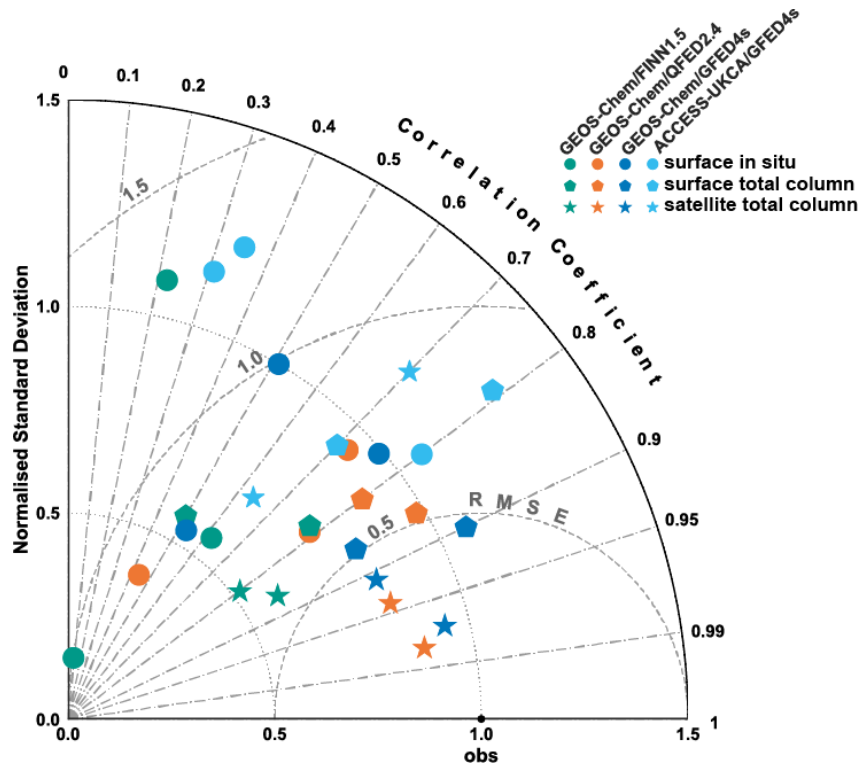


Figure 10. Taylor diagram summarising the evaluation of the four simulations against monthly mean surface in-situ (circles), surface total column (hexagons), and regional average MOPITT satellite (stars) measurements. Evaluation metrics include the normalised standard deviation (radial coordinate, normalised to the observed standard deviation), correlation coefficient (angular coordinate), and root mean square error (RMSE; dashed semi-circles). The black dot labelled “obs” denotes the ideal performance (identical to the observations).

736 elling studies. The results from this study have motivated in part updates to the next
737 version of FINN (version 2, in preparation) and future evaluation is recommended when
738 that version is released.

739 5 Conclusions

740 Emissions from Australian biomass burning are a primary driver of seasonal and
741 interannual variability in Australian atmospheric composition but remain highly uncer-
742 tain due to a dearth of measurements in the unique Australian environment. In this work,
743 we used surface in situ, ground-based total column, and satellite total column observa-
744 tions to evaluate the ability of two global atmospheric chemistry models (GEOS-Chem
745 and ACCESS-UKCA) and three global biomass burning emission inventories (FINN1.5,
746 GFED4s, and QFED2.4) to simulate CO in the Australian atmosphere from 2008 to 2010.

747 Comparison of CO emissions from the three inventories showed that FINN1.5 es-
748 timates substantially lower emissions than the other two inventories, particularly in the
749 northern Australia savanna. Estimates from GFED4s and QFED2.4 are similar in sea-
750 sonality to one another but with higher magnitude in QFED2.4. On a hemispheric scale,
751 the Australian emissions are dwarfed by emissions from Africa and South America, with
752 Australia responsible for 1-15% of total Southern Hemisphere fire emissions, complicat-
753 ing the interpretation of the Australian evaluation.

754 Of the existing observational datasets, we found that only the Darwin surface in
755 situ record provides information on fresh biomass burning emissions from Australian sa-
756 vanna fires. Here, GEOS-Chem significantly underestimated the CO surface mixing ra-
757 tios and reproduced little of the observed variability on either hourly or monthly timescales,
758 irrespective of the biomass burning inventory used. ACCESS-UKCA, on the other hand,
759 simulated Darwin surface CO to within 2% of the observed mean and reproduced nearly
760 two thirds of the observed seasonal variability, with the difference between the two mod-
761 els attributable to the finer horizontal resolution of ACCESS-UKCA.

762 Elsewhere, the existing measurements in both northern and southern Australia are
763 primarily sensitive to background CO and aged smoke. The simulations overestimated
764 the CO background at these sites (with the exception of ACCESS-UKCA at Wollongong),
765 hindering evaluation of the biomass burning inventories. Although the inventories dif-
766 fered substantially in terms of the magnitude of Australian emissions (Section 3), the
767 relative impacts of the bias in background CO versus the bias in Australian biomass burn-
768 ing CO could not be disentangled.

769 Evaluation therefore focused on the ability of each simulation to reproduce the ob-
770 served variability. Comparing the two models driven by the same inventory (GFED4s),
771 GEOS-Chem captured more of the observed variability at the remote sites than ACCESS-
772 UKCA, perhaps due to the more complex chemical mechanism (which would influence
773 the secondary production and loss of CO). Amongst the three GEOS-Chem simulations,
774 GFED4s and QFED2.4 performed similarly. The simulation with FINN1.5 was notably
775 worse, particularly at Darwin where almost no seasonal variability was simulated, high-
776 lighting insufficient emissions from savanna fires in FINN1.5. Only GFED4s captured
777 the enhanced CO at Wollongong from the Black Saturday event; however, the GFED4s
778 simulations overestimated CO at Cape Grim during this event, implying the emissions
779 associated with the event may be overestimated in GFED4s. Overall, we recommend that
780 global CO modelling studies with focus on Australia and/or the Southern Hemisphere
781 use GFED4s emissions rather than QFED2.4 (which leads to large biases when coupled
782 with the existing biases in the CO background) or FINN1.5 (which underestimates ob-
783 served variability).

784 Our results also showed that existing observations in Australia can only partially
785 constrain global model estimates of biomass burning. Only the Darwin surface in situ

786 measurements are sensitive to fresh fire emissions, but simulation of CO from these emis-
 787 sions is highly sensitive to model resolution. Meanwhile, the total column CO measure-
 788 ments at Darwin and Wollongong are less sensitive to resolution and boundary layer ef-
 789 fects but are significantly impacted by transported smoke from large emissions upwind
 790 in Africa and South America. Preliminary evaluation using shorter-lived formaldehyde
 791 at Wollongong provided no additional insight, as there was virtually no difference be-
 792 tween formaldehyde simulated at Wollongong using the three different inventories (not
 793 shown here). While formaldehyde has not previously been measured systematically at
 794 Darwin, recent equipment upgrades will provide a formaldehyde total column record in
 795 future, which we expect to provide more useful constraints on biomass burning emissions
 796 from Australian savanna fires.

797 Australian fires are a key contributor to global carbon emissions (Shi et al., 2015;
 798 van der Werf et al., 2017; Prospero et al., 2020) and to Australia’s carbon budget (Haverd
 799 et al., 2013, 2015). Climate change is increasing the risk of extreme fire seasons in Aus-
 800 tralia (van Oldenborgh et al., 2021), with potentially significant augmentation of car-
 801 bon emissions as seen during the recent 2019-2020 megafires (Shiraishi & Hirata, 2021).
 802 At the same time, more frequent fires may be reducing the carbon stores and associated
 803 fire emissions from Australia’s southeastern forests (Bowman et al., 2020), and adoption
 804 of Aboriginal fire management practices are already decreasing fire frequency and po-
 805 tentially emissions from the northern savannas (Ansell et al., 2020; Liu et al., 2021). Im-
 806 plementing these ongoing environmental and management changes into the next gener-
 807 ation of global biomass burning emission inventories is a key priority for accurately sim-
 808 ulating Australian fire emissions and their regional and global impacts.

809 Acronyms

810 **ACCESS-UKCA** Australian Community Climate and Earth System Simulator - United
 811 Kingdom Chemistry and Aerosol
 812 **ECMWF** European Centre for Medium-Range Weather Forecasts
 813 **FINN1.5** Fire INventory from NCAR version 1.5
 814 **GEOS** Goddard Earth Observing System
 815 **GFED4s** Global Fire Emissions Dataset version 4s
 816 **MODIS** Moderate Resolution Imaging Spectroradiometer
 817 **MOPITT** Measurements Of Pollution In The Troposphere
 818 **QFED2.4** Quick Fire Emissions Dataset version 2.4

819 Acknowledgments

820 We gratefully acknowledge Clare Paton-Walsh for helpful comments on the manuscript.
 821 This work was funded in part by ARC Discovery Project DP160101598 and was under-
 822 taken with the assistance of resources provided at the National Computational Infras-
 823 tructure (NCI) National Facility systems at the Australian National University through
 824 the National Computational Merit Allocation Scheme (project m19) supported by the
 825 Australian Government. The ACCESS model development was supported by funding
 826 from the Australian Climate Change Science Programme (ACCSP), and the model sim-
 827 ulations were made with the assistance of resources and services from the NCI, which
 828 is supported by the Australian government. Martin Dix and Scott Wales are acknowl-
 829 edged for their help with the ACCESS model setup. The NCAR MOPITT project is sup-
 830 ported by the NASA Earth Observing System (EOS) Program. Dr Maximilien Desservet-
 831 taz was supported during this work by a CSIRO Office of the Chief Executive Postgrad-
 832 uate Scholarship. CSIRO is thanked for the long-term support of the CSIRO GASLAB
 833 flask network, including Cape Ferguson. The Cape Grim in situ CO measurements are

834 supported by the Australian Bureau of Meteorology, CSIRO, and the National Aeronau-
835 tics and Space Administration (grant no. NNX16AC98G).

836 In situ CO data at Darwin are available from the corresponding author by request.
837 In situ data for Cape Grim were provided by Dr. P Krummel of CSIRO’s Climate Sci-
838 ence Centre and are available upon request. In situ data at Cape Ferguson were down-
839 loaded from the World Data Centre for Greenhouse Gases webpage ([https://gaw.kishou](https://gaw.kishou.go.jp/search/station#CFA)
840 [.go.jp/search/station#CFA](https://gaw.kishou.go.jp/search/station#CFA)). Ground-based total column at Wollongong were down-
841 loaded from the NDACC network database ([https://ftp.cpc.ncep.noaa.gov/ndacc/](https://ftp.cpc.ncep.noaa.gov/ndacc/station/wollong/)
842 [station/wollong/](https://ftp.cpc.ncep.noaa.gov/ndacc/station/wollong/)). Ground-based total column data at Darwin were downloaded from
843 the TCCON network database (<https://data.caltech.edu/records/291>). MOPITT
844 Version 7 level 3 data were obtained from the NASA data archive ([https://15eil01](https://15eil01.larc.nasa.gov:22000/distribution/pub/MOPITT/MOP03JM.007/)
845 [.larc.nasa.gov:22000/distribution/pub/MOPITT/MOP03JM.007/](https://15eil01.larc.nasa.gov:22000/distribution/pub/MOPITT/MOP03JM.007/)). Information to
846 download, install and run GEOS-Chem is available Harvard’s wiki page [http://wiki](http://wiki.seas.harvard.edu/geos-chem/index.php/Main_Page)
847 [.seas.harvard.edu/geos-chem/index.php/Main_Page](http://wiki.seas.harvard.edu/geos-chem/index.php/Main_Page). Set-up files for this study and
848 analysis codes (python) of the output files are available in Github [https://github.com/](https://github.com/jennyfisher/AusBBemissionsPaper)
849 [jennyfisher/AusBBemissionsPaper](https://github.com/jennyfisher/AusBBemissionsPaper).

850 References

- 851 Abraham, N. L., Archibald, A. T., Bellouin, N., Boucher, O., Braesicke, P., Bushell,
852 A., ... others (2012). Unified model documentation paper no. 84: United
853 Kingdom Chemistry and Aerosol (UKCA) technical description MetUM ver-
854 sion 8.2. *UK Met Office, Exeter, UK*.
- 855 Akagi, S. K., Yokelson, R. J., Wiedinmyer, C., Alvarado, M. J., Reid, J. S., Karl, T.,
856 ... Wennberg, P. O. (2011). Emission factors for open and domestic biomass
857 burning for use in atmospheric models. *Atmospheric Chemistry and Physics*,
858 *11*(9), 4039-4072.
- 859 Andreae, M. O., & Merlet, P. (2001). Emission of trace gases and aerosols from
860 biomass burning. *Global Biogeochemical Cycles*, *15*(4), 955–966.
- 861 Ansell, J., Evans, J., Rangers, A., Rangers, A. S., Rangers, D., Rangers, J., ...
862 Rangers, Y. M. (2020). Contemporary Aboriginal savanna burning projects
863 in Arnhem Land: a regional description and analysis of the fire management
864 aspirations of Traditional Owners. *International Journal of Wildland Fire*,
865 *29*(5), 371.
- 866 Bey, I., Jacob, D. J., Yantosca, R. M., Logan, J. A., Field, B. D., Fiore, A. M., ...
867 Schultz, M. G. (2001). Global modeling of tropospheric chemistry with assim-
868 ilated meteorology: Model description and evaluation. *Journal of Geophysical*
869 *Research: Atmospheres*, *106*(D19), 23073–23095.
- 870 Bi, D., Dix, M., Marsland, S. J., O’Farrell, S., Rashid, H., Uotila, P., ... others
871 (2013). The ACCESS coupled model: description, control climate and evalua-
872 tion. *Australian Meteorological and Oceanographic Journal*, *63*(1), 41–64.
- 873 Bowman, D. M., Williamson, G. J., Price, O. F., Ndalila, M. N., & Bradstock, R. A.
874 (2020). Australian forests megafires and the risk of dwindling carbon stocks.
875 *Plant, Cell & Environment*, *44*(2), 347–355.
- 876 BrisbaneTimes. (2008). *Tassie fires ‘can be seen from victoria’*. Retrieved 2021-
877 09-24, from [https://www.brisbanetimes.com.au/national/queensland/](https://www.brisbanetimes.com.au/national/queensland/tassie-fires-can-be-seen-from-victoria-20080320-ge9s9n.html)
878 [tassie-fires-can-be-seen-from-victoria-20080320-ge9s9n.html](https://www.brisbanetimes.com.au/national/queensland/tassie-fires-can-be-seen-from-victoria-20080320-ge9s9n.html)
- 879 Buchholz, R. R., Deeter, M. N., Worden, H. M., Gille, J., Edwards, D. P., Hannigan,
880 J. W., ... Langerock, B. (2017). Validation of MOPITT carbon monoxide us-
881 ing ground-based Fourier transform infrared spectrometer data from NDACC.
882 *Atmospheric Measurement Techniques*, *10*(5), 1927.
- 883 Buchholz, R. R., Hammerling, D., Worden, H. M., Deeter, M. N., Emmons, L. K.,
884 Edwards, D. P., & Monks, S. A. (2018). Links between carbon monoxide and
885 climate indices for the southern hemisphere and tropical fire regions. *Journal*

- 886 *of Geophysical Research: Atmospheres*, 123(17), 9786–9800.
- 887 Buchholz, R. R., Paton-Walsh, C., Griffith, D. W. T., Kubistin, D., Caldow, C.,
888 Fisher, J. A., ... Langenfelds, R. L. (2016). Source and meteorological influ-
889 ences on air quality (CO, CH₄ & CO₂) at a Southern Hemisphere urban site.
890 *Atmospheric Environment*, 126, 274–289.
- 891 Cook, G., Hurst, D. F., & Griffith, D. W. (1995). Atmospheric trace gas emissions
892 from tropical australian savanna fires. *CALMscience*, 123–128.
- 893 Cruz, M. G., Sullivan, A. L., Gould, J. S., Sims, N. C., Bannister, A. J., Hollis, J. J.,
894 & Hurley, R. J. (2012). Anatomy of a catastrophic wildfire: the Black Satur-
895 day Kilmore East fire in Victoria, Australia. *Forest Ecology and Management*,
896 284, 269–285.
- 897 Darnenov, A., & da Silva, A. (2015). The Quick Fire Emissions Dataset (QFED)–
898 documentation of versions 2.1, 2.2 and 2.4. *NASA Technical Report Series on*
899 *Global Modeling and Data Assimilation*, 38, 199.
- 900 Dee, D. P., Uppala, S. M., Simmons, A., Berrisford, P., Poli, P., Kobayashi, S., ...
901 others (2011). The era-interim reanalysis: Configuration and performance of
902 the data assimilation system. *Quarterly Journal of the royal meteorological*
903 *society*, 137(656), 553–597.
- 904 Deeter, M. N., Edwards, D. P., Francis, G. L., Gille, J. C., Martínez-Alonso, S.,
905 Worden, H. M., & Sweeney, C. (2017). A climate-scale satellite record for
906 carbon monoxide: the mopitt version 7 product. *Atmospheric Measurement*
907 *Techniques*, 10(7), 2533–2555.
- 908 Desservettaz, M., Paton-Walsh, C., Griffith, D. W. T., Kettlewell, G., Keywood,
909 M. D., Vanderschoot, M. V., ... Atkinson, B. (2017). Emission factors of trace
910 gases and particles from tropical savanna fires in Australia. *Journal of Geo-*
911 *physical Research: Atmospheres*, 122, 6059–2074. doi: 10.1002/2016JD025925
- 912 Deutscher, N., Griffith, D., Bryant, G., Wennberg, P., Toon, G., Washenfelder, R.,
913 ... Park, S. (2010). Total column CO₂ measurements at Darwin, Australia-
914 site description and calibration against in situ aircraft profiles. *Atmospheric*
915 *Measurement Techniques*, 3(4), 947–958. doi: 10.5194/amt-3-947-2010
- 916 Drummond, J. R., & Mand, G. S. (1996). The Measurements of Pollution in the
917 Troposphere (MOPITT) instrument: Overall performance and calibration re-
918 quirements. *Journal of Atmospheric and Oceanic Technology*, 13(2), 314–320.
- 919 Eastham, S. D., & Jacob, D. J. (2017). Limits on the ability of global Eulerian
920 models to resolve intercontinental transport of chemical plumes. *Atmospheric*
921 *Chemistry and Physics*, 17(4), 2543–2553. doi: 10.5194/acp-17-2543-2017
- 922 Edwards, D. P., Emmons, L. K., Gille, J. C., Chu, A., Attié, J.-L., Giglio, L., ...
923 Drummond, J. R. (2006). Satellite-observed pollution from Southern Hemi-
924 sphere biomass burning. *Journal of Geophysical Research*, 111(D14). doi:
925 10.1029/2005jd006655
- 926 Emmons, L. K., Edwards, D. P., Deeter, M. N., Gille, J. C., Campos, T., Nédélec,
927 P., ... Sachse, G. (2009). Measurements of Pollution in the Troposphere (MO-
928 PITT) validation through 2006. *Atmospheric Chemistry and Physics*, 9(5),
929 1795–1803.
- 930 Eyring, V., Köhler, H. W., Van Aardenne, J., & Lauer, A. (2005). Emissions from
931 international shipping: 1. The last 50 years. *Journal of Geophysical Research:*
932 *Atmospheres*, 110(D17).
- 933 Field, C. B., Randerson, J. T., & Malmström, C. M. (1995). Global net primary
934 production: Combining ecology and remote sensing. *Remote Sensing of Envi-*
935 *ronment*, 51(1), 74–88.
- 936 Fisher, J. A., Murray, L. T., Jones, D. B. A., & Deutscher, N. M. (2017). Improved
937 method for linear carbon monoxide simulation and source attribution in at-
938 mospheric chemistry models illustrated using GEOS-Chem v9. *Geoscientific*
939 *Model Development*, 10(11), 4129–4144.
- 940 Giglio, L., Randerson, J. T., & van der Werf, G. R. (2013). Analysis of daily

- 941 monthly, and annual burned area using the fourth-generation global fire emis-
 942 sions database (GFED4). *Journal of Geophysical Research: Biogeosciences*,
 943 *118*(1), 317–328. doi: 10.1002/jgrg.20042
- 944 Gill, A. M. (1975). Fire and the Australian flora: a review. *Australian forestry*,
 945 *38*(1), 4–25.
- 946 Griffith, D., Deutscher, N., Velazco, V., Wennberg, P., Yavin, Y., Keppel-Aleks, G.,
 947 ... others (2014). *Tccon data from darwin (au), release ggg2014* (Vol. 10).
 948 doi: <http://dx.doi.org/10.14291/tccon.ggg2014.darwin01.R0/1149290>
- 949 Griffith, D. W. T., Deutscher, N. M., Caldow, C., Kettlewell, G., Riggenbach, M.,
 950 & Hammer, S. (2012). A Fourier transform infrared trace gas and isotope
 951 analyser for atmospheric applications. *Atmospheric Measurement Techniques*,
 952 *5*(10), 2481–2498.
- 953 Guenther, A. B., Jiang, X., Heald, C. L., Sakulyanontvittaya, T., Duhl, T., Em-
 954 mons, L. K., & Wang, X. (2012). The Model of Emissions of Gases and
 955 Aerosols from Nature version 2.1 (MEGAN2.1): an extended and updated
 956 framework for modeling biogenic emissions. *Geoscientific Model Development*,
 957 *5*(6), 1471–1492. doi: 10.5194/gmd-5-1471-2012
- 958 Haverd, V., Raupach, M. R., Briggs, P. R., Canadell, J. G., Davis, S. J., Law,
 959 R. M., ... Sherman, B. (2013). The Australian terrestrial carbon budget.
 960 *Biogeosciences*, *10*(2), 851–869. doi: 10.5194/bg-10-851-2013
- 961 Haverd, V., Raupach, M. R., Briggs, P. R., Canadell, J. G., Davis, S. J., Law,
 962 R. M., ... Sherman, B. (2015). Corrigendum to “The Australian Terres-
 963 trial Carbon Budget” published in *Biogeosciences* 10, 851–869, 2013. *Biogeo-*
 964 *sciences*, *12*(11), 3603–3605. doi: 10.5194/bg-12-3603-2015
- 965 Hoelzemann, J. J., Schultz, M. G., Brasseur, G. P., Granier, C., & Simon, M.
 966 (2004). Global Wildland Fire Emission Model (GWEM): Evaluating the
 967 use of global area burnt satellite data. *Journal of Geophysical Research: Atmo-*
 968 *spheres*, *109*(D14).
- 969 Hurst, D. F., Griffith, D. W. T., Carras, J. N., Williams, D. J., & Fraser, P. J.
 970 (1994). Measurements of trace gases emitted by Australian savanna fires
 971 during the 1990 dry season. *Journal of Atmospheric Chemistry*, *18*(1), 33–56.
- 972 Hurst, D. F., Griffith, D. W. T., & Cook, G. D. (1994). Trace Gas Emissions from
 973 Biomass Burning in Tropical Australian Savannas. *Journal of Geophysical*
 974 *Research-Atmospheres*, *99*(D8), 16441–16456.
- 975 Khalil, M., & Rasmussen, R. (1984). Carbon monoxide in the earth’s atmosphere:
 976 increasing trend. *Science*, *224*(4644), 54–56.
- 977 Krummel, P., Langenfelds, R., & Loh, Z. (2016). *Atmospheric CO at Cape Fergu-*
 978 *son by Commonwealth Scientific and Industrial Research Organisation, dataset*
 979 *published as CO-CFA_surface-flask-CSIRO_data1 at WDCGG, ver. 2021-0408-*
 980 *1004*. doi: 10.50849/WDCGG_0016-5010-3001-01-02-9999
- 981 Lamarque, J.-F., Shindell, D. T., Josse, B., Young, P. J., Cionni, I., Eyring, V., ...
 982 others (2013). The Atmospheric Chemistry and Climate Model Intercompar-
 983 ison Project (ACCMIP): overview and description of models, simulations and
 984 climate diagnostics. *Geoscientific Model Development*, *6*, 179–206.
- 985 Langenfelds, R., Francey, R., Pak, B., Steele, L., Lloyd, J., Trudinger, C., & Allison,
 986 C. (2002). Interannual growth rate variations of atmospheric co2 and its $\delta^{13}C$,
 987 h2, ch4, and co between 1992 and 1999 linked to biomass burning. *Global*
 988 *Biogeochemical Cycles*, *16*(3), 21–1.
- 989 Law, R. M., Steele, L. P., Krummel, P. B., & Zahorowski, W. (2010). Synoptic
 990 variations in atmospheric co2 at cape grim: a model intercomparison. *Tellus B:*
 991 *Chemical and Physical Meteorology*, *62*(5), 810–820.
- 992 Lewis, S. L., Brando, P. M., Phillips, O. L., van der Heijden, G. M. F., & Nepstad,
 993 D. (2011). The 2010 Amazon Drought. *Science*, *331*(6017), 554–554. doi:
 994 10.1126/science.1200807
- 995 Lieschke, K. J., Fisher, J. A., Paton-Walsh, C., Jones, N. B., Greenslade, J. W.,

- 996 Burden, S., & Griffith, D. W. T. (2019). Decreasing Trend in Formaldehyde
997 Detected From 20-Year Record at Wollongong Southeast Australia. *Geophysical*
998 *Research Letters*, *46*(14), 8464–8473. doi: 10.1029/2019gl083757
- 999 Liu, T., Mickley, L. J., Marlier, M. E., DeFries, R. S., Khan, M. F., Latif, M. T., &
1000 Karambelas, A. (2020). Diagnosing spatial biases and uncertainties in global
1001 fire emissions inventories: Indonesia as regional case study. *Remote Sensing of*
1002 *Environment*, *237*, 111557. doi: 10.1016/j.rse.2019.111557
- 1003 Liu, T., Mickley, L. J., & McCarty, J. L. (2021). Global search for temporal shifts in
1004 fire activity: potential human influence on southwest russia and north australia
1005 fire seasons. *Environmental Research Letters*, *16*(4), 044023.
- 1006 Loh, Z., Law, R., Haynes, K., Krummel, P., Steele, L., Fraser, P., . . . Williams, A.
1007 (2015). Simulations of atmospheric methane for cape grim, tasmania, to con-
1008 strain southeastern australian methane emissions. *Atmospheric Chemistry and*
1009 *Physics*, *15*(1), 305–317.
- 1010 Naik, V., Voulgarakis, A., Fiore, A. M., Horowitz, L. W., Lamarque, J.-F., Lin,
1011 M., . . . others (2013). Preindustrial to present-day changes in tropospheric
1012 hydroxyl radical and methane lifetime from the atmospheric chemistry and
1013 climate model intercomparison project (accmip). *Atmospheric Chemistry and*
1014 *Physics*, *13*(10), 5277–5298.
- 1015 NASA/LARC/SD/ASDC. (n.d.). *Mopitt co gridded monthly means (near and ther-*
1016 *mal infrared radiances) v007*. NASA Langley Atmospheric Science Data Center
1017 DAAC. Retrieved from [https://doi.org/10.5067/TERRA/MOPITT/MOP03JM](https://doi.org/10.5067/TERRA/MOPITT/MOP03JM_L3.007)
1018 [_L3.007](https://doi.org/10.5067/TERRA/MOPITT/MOP03JM_L3.007)
- 1019 Olivier, J. G., Peters, J. A., Bakker, J., Berdowski, J. J., Visschedijk, A. J., & Bloos,
1020 J. P. (2002, Jul). *Applications of edgar. including a description of edgar 3.2.*
1021 *reference database with trend data for 1970-1995*.
- 1022 Pan, X., Ichoku, C., Chin, M., Bian, H., Darmenov, A., Colarco, P., . . . Cui, G.
1023 (2020). Six global biomass burning emission datasets: intercomparison and
1024 application in one global aerosol model. *Atmospheric Chemistry and Physics*,
1025 *20*(2), 969–994.
- 1026 Paton-Walsh, C., Deutscher, N. M., Griffith, D. W. T., Forgan, B. W., Wilson,
1027 S. R., Jones, N. B., & Edwards, D. P. (2010). Trace gas emissions from sa-
1028 vanna fires in northern Australia. *Journal of Geophysical Research*, *115*(D16).
1029 doi: 10.1029/2009jd013309
- 1030 Paton-Walsh, C., Emmons, L. K., & Wiedinmyer, C. (2012). Australia’s
1031 Black Saturday fires—Comparison of techniques for estimating emissions
1032 from vegetation fires. *Atmospheric Environment*, *60*, 262–270. doi:
1033 10.1016/j.atmosenv.2012.06.066
- 1034 Paugam, R., Wooster, M., Freitas, S., & Val Martin, M. (2016). A review of ap-
1035 proaches to estimate wildfire plume injection height within large-scale atmo-
1036 spheric chemical transport models. *Atmospheric Chemistry and Physics*, *16*(2),
1037 907–925.
- 1038 Potter, C. S., Randerson, J. T., Field, C. B., Matson, P. A., Vitousek, P. M.,
1039 Mooney, H. A., & Klooster, S. A. (1993). Terrestrial ecosystem production: A
1040 process model based on global satellite and surface data. *Global Biogeochemical*
1041 *Cycles*, *7*(4), 811–841.
- 1042 Prinn, R. G., Weiss, R. F., Arduini, J., Arnold, T., DeWitt, H. L., Fraser, P. J., . . .
1043 others (2018). History of chemically and radiatively important atmospheric
1044 gases from the advanced global atmospheric gases experiment (agage). *Earth*
1045 *System Science Data*, *10*(2), 985–1018.
- 1046 Prospero, P., Bloise, M., Tubiello, F. N., Conchedda, G., Rossi, S., Boschetti, L., . . .
1047 Bernoux, M. (2020). New estimates of greenhouse gas emissions from biomass
1048 burning and peat fires using MODIS Collection 6 burned areas. *Climatic*
1049 *Change*, *161*(3), 415–432. doi: 10.1007/s10584-020-02654-0
- 1050 Randerson, J. T., Chen, Y., van der Werf, G. R., Rogers, B. M., & Morton, D. C.

- 1051 (2012). Global burned area and biomass burning emissions from small
 1052 fires. *Journal of Geophysical Research: Biogeosciences*, *117*(G4). doi:
 1053 10.1029/2012jg002128
- 1054 Randerson, J. T., Thompson, M. V., Malmstrom, C. M., Field, C. B., & Fung, I. Y.
 1055 (1996). Substrate limitations for heterotrophs: Implications for models that
 1056 estimate the seasonal cycle of atmospheric CO₂. *Global Biogeochemical Cycles*,
 1057 *10*(4), 585–602. doi: 10.1029/96gb01981
- 1058 Rastigejev, Y., Park, R., Brenner, M. P., & Jacob, D. J. (2010). Resolving intercon-
 1059 tinental pollution plumes in global models of atmospheric transport. *Journal of*
 1060 *Geophysical Research*, *115*(D2). doi: 10.1029/2009jd012568
- 1061 Rea, G., Paton-Walsh, C., Turquety, S., Cope, M., & Griffith, D. (2016). Impact
 1062 of the New South Wales fires during October 2013 on regional air quality in
 1063 eastern Australia. *Atmospheric Environment*, *131*, 150–163.
- 1064 Reinhart, W., & Millet, D. (2011). Implementation of the RETRO Anthropogenic
 1065 Emission Inventory into the GEOS-Chem Model. *University of Minnesota*.
- 1066 Rodgers, C. D., & Connor, B. J. (2003). Intercomparison of remote sounding instru-
 1067 ments. *Journal of Geophysical Research: Atmospheres*, *108*(D3). doi: 10.1029/
 1068 2002jd002299
- 1069 Russell-Smith, J., Yates, C. P., Whitehead, P. J., Smith, R., Craig, R., Allan, G. E.,
 1070 ... Gill, A. M. (2007). Bushfires ‘down under’: patterns and implications of
 1071 contemporary Australian landscape burning. *International Journal of Wildland*
 1072 *Fire*, *16*(4), 361–377. doi: 10.1071/WF07018
- 1073 Seiler, W., & Crutzen, P. J. (1980). Estimates of gross and net fluxes of carbon
 1074 between the biosphere and the atmosphere from biomass burning. *Climatic*
 1075 *Change*, *2*(3), 207–247.
- 1076 Shi, Y., Matsunaga, T., Saito, M., Yamaguchi, Y., & Chen, X. (2015). Comparison
 1077 of global inventories of CO₂ emissions from biomass burning during 2002–
 1078 2011 derived from multiple satellite products. *Environmental Pollution*, *206*,
 1079 479–487.
- 1080 Shiraishi, T., & Hirata, R. (2021). Estimation of carbon dioxide emissions from the
 1081 megafires of Australia in 2019–2020. *Scientific Reports*, *11*(1). doi: 10.1038/
 1082 s41598-021-87721-x
- 1083 Siddaway, J. M., & Petelina, S. V. (2011). Transport and evolution of the 2009
 1084 Australian Black Saturday bushfire smoke in the lower stratosphere ob-
 1085 served by OSIRIS on Odin. *Journal of Geophysical Research*, *116*(D6). doi:
 1086 10.1029/2010jd015162
- 1087 Simone, N. W., Stettler, M. E. J., & Barrett, S. R. H. (2013). Rapid estimation of
 1088 global civil aviation emissions with uncertainty quantification. *Transportation*
 1089 *Research Part D: Transport and Environment*, *25*, 33–41.
- 1090 Sindelarova, K., Granier, C., Bouarar, I., Guenther, A., Tilmes, S., Stavrakou, T.,
 1091 ... Knorr, W. (2014). Global data set of biogenic VOC emissions calculated
 1092 by the MEGAN model over the last 30 years. *Atmospheric Chemistry and*
 1093 *Physics*, *14*(17), 9317–9341.
- 1094 van der Werf, G. R., Randerson, J. T., Giglio, L., van Leeuwen, T. T., Chen, Y.,
 1095 Rogers, B. M., ... Kasibhatla, P. S. (2017). Global fire emissions estimates
 1096 during 1997–2016. *Earth System Science Data*, *9*(2), 697–720.
- 1097 van Oldenborgh, G. J., Krikken, F., Lewis, S., Leach, N. J., Lehner, F., Saunders,
 1098 K. R., ... Otto, F. E. L. (2021). Attribution of the Australian bushfire risk
 1099 to anthropogenic climate change. *Natural Hazards and Earth System Sciences*,
 1100 *21*(3), 941–960. doi: 10.5194/nhess-21-941-2021
- 1101 Wai, K. M., Wu, S., Kumar, A., & Liao, H. (2014). Seasonal variability and long-
 1102 term evolution of tropospheric composition in the tropics and Southern Hemi-
 1103 sphere. *Atmospheric Chemistry and Physics*, *14*(10), 4859.
- 1104 Wiedinmyer, C., Akagi, S. K., Yokelson, R. J., Emmons, L. K., Al-Saadi, J. A., Or-
 1105 lando, J. J., & Soja, A. J. (2011). The Fire INventory from NCAR (FINN):

- 1106 A high resolution global model to estimate the emissions from open burning.
1107 *Geoscientific Model Development*, 4, 625.
- 1108 Woodhouse, M. T., Luhar, A. K., Stevens, L., Galbally, I., Thatcher, M., Uhe, P.,
1109 ... Molloy, S. (2015). Australian reactive-gas emissions in a global chemistry-
1110 climate model and initial results. *Air Quality and Climate Change*, 49(4),
1111 31–38.
- 1112 Woodruff, S. D., Worley, S. J., Lubker, S. J., Ji, Z., Freeman, E. J., Berry, D. I., ...
1113 others (2011). ICOADS Release 2.5: extensions and enhancements to the
1114 surface marine meteorological archive. *International Journal of Climatology*,
1115 31(7), 951–967. doi: 10.1002/joc.2103
- 1116 Wooster, M. J. (2002). Small-scale experimental testing of fire radiative energy for
1117 quantifying mass combusted in natural vegetation fires. *Geophysical Research*
1118 *Letters*, 29(21). doi: 10.1029/2002gl015487
- 1119 Wooster, M. J., Roberts, G., Perry, G. L. W., & Kaufman, Y. J. (2005). Retrieval
1120 of biomass combustion rates and totals from fire radiative power observations:
1121 FRP derivation and calibration relationships between biomass consumption
1122 and fire radiative energy release. *Journal of Geophysical Research*, 110(D24).
1123 doi: 10.1029/2005jd006318
- 1124 Worden, H., Deeter, M., Edwards, D., Gille, J., Drummond, J., & Nédélec, P.
1125 (2010). Observations of near-surface carbon monoxide from space using mo-
1126 pitt multispectral retrievals. *Journal of Geophysical Research: Atmospheres*,
1127 115(D18).
- 1128 Yevich, R., & Logan, J. A. (2003). An assessment of biofuel use and burning of agri-
1129 cultural waste in the developing world. *Global Biogeochemical Cycles*, 17(4).
- 1130 Zeng, G., Williams, J. E., Fisher, J. A., Emmons, L. K., Jones, N. B., Morgenstern,
1131 O., ... Griffith, D. W. T. (2015). Multi-model simulation of CO and HCHO
1132 in the Southern Hemisphere: comparison with observations and impact of bio-
1133 genic emissions. *Atmospheric Chemistry and Physics*, 15, 7217–7245. doi:
1134 10.5194/acp-15-7217-2015